# TECHNICAL REPORT R-60

---

# A STUDY OF SOME FACTORS AFFECTING
# ROLLING-CONTACT FATIGUE LIFE

By THOMAS L. CARTER

Lewis Research Center
Cleveland, Ohio

# CONTENTS

# TECHNICAL REPORT R-60

## A STUDY OF SOME FACTORS AFFECTING ROLLING-CONTACT FATIGUE LIFE[1]

By Thomas L. Carter

### SUMMARY

*A series of investigations using the fatigue spin rig to study the effect of several factors contributing to rolling-contact fatigue life is summarized. Ball specimens of ½- and %₁₆-inch diameter were tested at maximum theoretical Hertz compressive stresses in the range of 600,000 to 750,000 psi.*

*Life was found to vary inversely with the tenth power of stress. In forging fiber studies, a greater concentration of failures and poorer life were observed where the greatest angle of intersection between the fiber flow lines and the surface occurred. This effect was independent of alloy composition. Higher lubricant viscosity was found to increase fatigue life. Lubricants having the same viscosity but of different base stock produced wide differences in life that correlated with the pressure viscosity coefficient of the lubricant. Higher temperature produced lower fatigue life. Dry-powder lubricants produced poor fatigue life at 450° F; failure appearance indicated that the lubricant particles probably acted as minute stress raisers. In metallographic studies, nonmetallic inclusions were found to have a deleterious effect on fatigue life—the inclusion size, location, composition, and condition of the matrix being contributing factors; failures were by shear cracking in the subsurface zone of maximum shear stress and eventual propagation into a shallow surface spall. Vacuum melting improved fatigue life, although a general correlation between cleanliness and fatigue life was not found. Life results for ten different bearing materials are presented.*

### INTRODUCTION

Traditional materials and lubricants are no longer adequate to satisfy the ever increasing demands of powerplant designers for high-temperature, high-speed, high-load-capacity rolling-contact bearings. High-performance materials must be developed if bearings are not to become a limitation to continued powerplant development (refs. 1 to 4). Since, as a minimum requirement, the materials must perform at the design temperature, a preliminary selection can be made on the basis of such properties as hot hardness and dimensional stability for bearing materials, and thermal and oxidative stability for lubricant materials. The tool steels provide a large group of potential alloys possessing high-temperature properties, and many synthetic lubricants are available with good high-temperature properties.

In addition to high-temperature properties, the lubricants and materials used in advanced bearing applications must provide adequate service life. Rolling-contact bearings, if properly designed, installed, and lubricated, do not wear out by abrasion but fail by fatigue of the races and rolling elements. For this reason, a thorough evaluation of potential materials with respect to rolling-contact fatigue life is prerequisite to the specification of high-temperature bearing materials and lubricants.

Material fatigue is known to be statistical in nature (ref. 5). Because of the wide scatter in fatigue data, large groups of specimens need to be tested under identical conditions of stress and environment to obtain conclusive results. Obtaining fatigue lives by testing full-scale bearings is time-consuming and costly; therefore, it would be advantageous to use a simpler test with fewer and less complex variables. Simple fatigue tests such as rotating-beam or vibration tests do not duplicate the pattern of very high surface compression and subsurface shear stresses characteristic of rolling-contact loading. The fracture failure of common fatigue tests differs greatly in appearance from rolling-contact spall failures. Styri (ref. 6) found that simple bench fatigue tests do not produce the stress-life relation characteristics of

rolling-contact bearings. An empirically established relation of bearing life (life varies inversely as the ninth to tenth power of contact stress) is considered representative of normal bearing-fatigue experience by the bearing industry (ref. 7).

A simple bench test that would produce the rolling-contact stress pattern, the characteristic failure spall, and a stress-life relation characteristic of bearings was considered desirable from the standpoint of cost, time, and ease of isolating individual factors affecting bearing fatigue life. The rolling-contact fatigue rig (ref. 8) was developed to fill this need. This rig, by rolling two centrifugally loaded balls at high speed around a cylindrical race bore, produces a very high frequency of application of the same stress pattern existing in full-scale bearings. The accelerated failure time, fewer and simpler rolling elements, and control over the stress volume make this rig a useful tool for evaluating potential bearing materials and lubricants.

The work described in this report consists of (1) an evaluation of the rolling-contact fatigue spin rig as a valid research tool, and (2) a series of investigations of some individual factors affecting rolling-contact fatigue life. These factors include applied stress, forging fiber orientation, lubricant viscosity, lubricant composition (base stock), temperature, dry-powder lubricants, metallographic structure changes, origin and propagation of failures, and material alloy composition. This study is based on work conducted at the NASA Lewis Research Center since 1956. Some of the work has not been reported previously.

## APPARATUS

### TEST RIG

Figure 1 shows a cutaway view of the rolling-contact fatigue spin rig, which is described in detail in reference 8. Two test balls revolve in a horizontal plane on the bore of a test-cylinder race that is coated with a film of the test lubricant. Air at pressures up to 100 pounds per square inch is introduced through nozzles to drive the balls at high orbital speeds (30,000 rpm); this is the equivalent of $1.5 \times 10^6$ DN. The nozzle system and race cylinder are positioned by upper and lower cover plates fastened by three removable bolts. The rig assembly is supported from a rigid frame by three flexible cables. In order to keep

external constraint at a low value (achieve low critical frequencies), the drive air is introduced into the rig through a 6-foot-long metal hose.

### OPERATION

The two test balls separate and maintain relative positions 180° apart at orbital speeds above 150 rpm. High precessional forces hold this relative position in the plane of the nozzle system. The dynamics of rig operation are analyzed in detail in reference 8.

### LOADING

The only loading on the test specimens is that produced by centrifugal force. No contact is made with the test balls except by the race cylinder at the contact ellipse. Load (and stress) is controlled by adjusting rotational velocity of the balls. The load can exceed 700 pounds for a ½-inch steel ball revolving in a 3.5-inch-bore race cylinder at an orbital speed of 30,000 rpm. At this speed a maximum theoretical Hertz stress of approximately 750,000-psi compression is developed at the center of the contact ellipse.

### INSTRUMENTATION

Three instrumentation systems provide for speed measurement and control, temperature measurement and control, and failure detection and shutdown.

Orbital speed of the balls is measured by counting the pulses from a photoamplifier. The pulses are generated when the two test balls interrupt a light beam focused on the photocell (fig. 1). A voltage proportional to the frequency of the photocell output is fed into a Swartwout Controller that automatically regulates the drive-air pressure to maintain the desired orbital ball speed.

Temperature is measured with an iron-constantan thermocouple in contact with the top of the race cylinder (fig. 1). This is the closest practical location of a thermocouple with relation to the ball running track. A calibration with a thermocouple in the airstream surrounding the balls showed a variation of less than 2° from the test temperature. It can be assumed that the race, balls, and surrounding air are all maintained within a narrow temperature range. A second thermocouple contacting the cylinder top provides the signal for the automatic temperature controller. This controller blends room-temperature air with
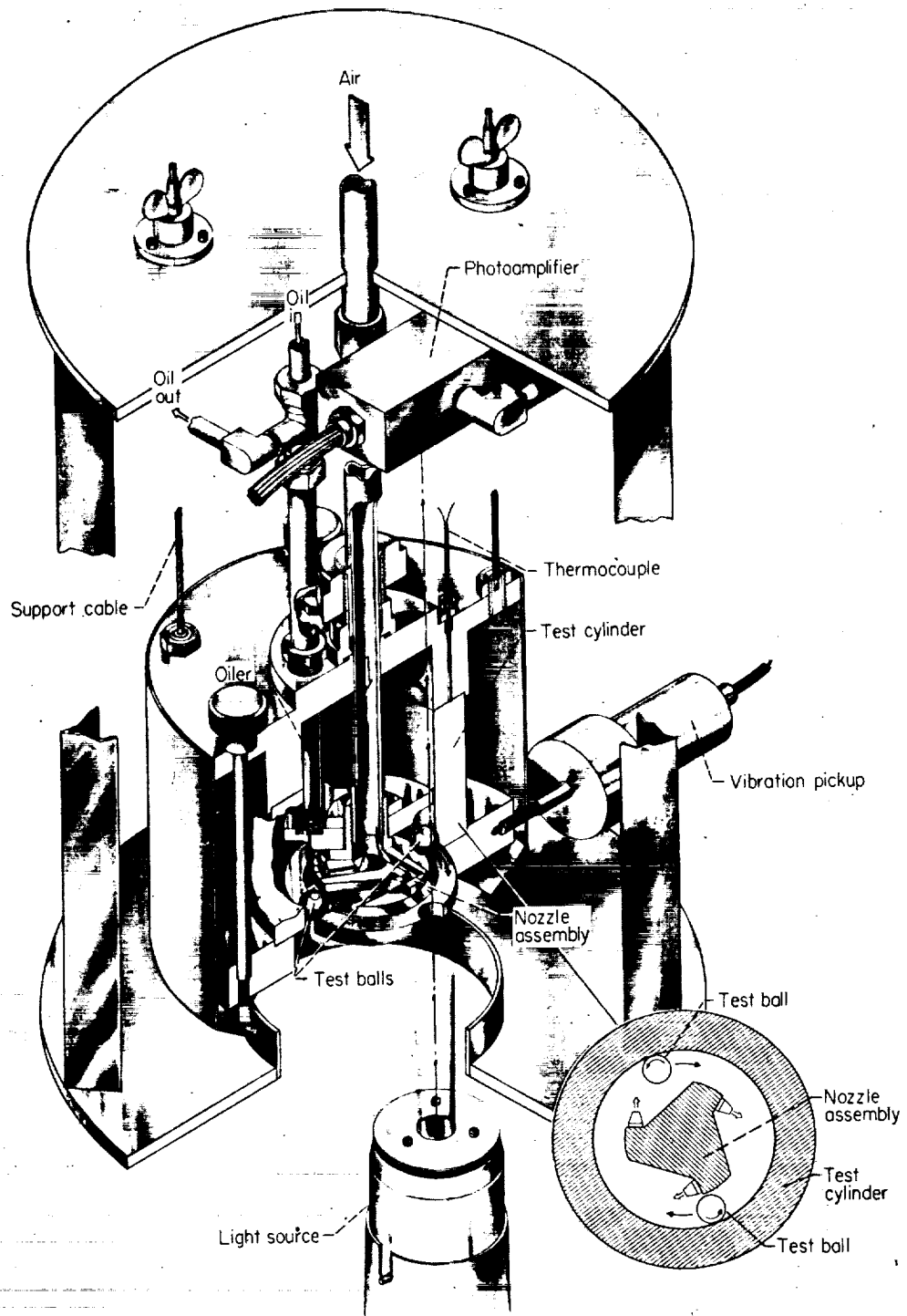
FIGURE 1.—Rolling-contact fatigue spin rig.

air heated by a 25-kilowatt heater in the proportion necessary to maintain the temperature of the drive-air supply at the desired level. This drive air surrounds the test balls and is then exhausted over the inner diameter of the race cylinder.

Failures are detected by comparing the amplified signal from a velocity vibration pickup (attached to the rig; see fig. 1) with a predetermined signal level preset on a meter relay. The large vibration amplitude resulting from a ball or cylinder fatigue spall trips the meter relay and results in shutdown of the test and all instrumentation.

### DRIVE-AIR SUPPLY

Drive air from a central supply at 125 pounds per square inch is dried to less than 30 percent relative humidity and is double filtered upstream from the control systems.

### LUBRICATION

The lubricant is introduced into the drive airstream between the guide plates (fig. 1). The rotating airstream forces the particles against the race surface to maintain a continuous film of fresh lubricant. Fluids and solid-fluid suspensions are metered by a pressure drop across a capillary tube. Dry powders are metered by a dust generator. Flow rates of approximately 5 milliliters per hour of fluids and suspensions and 10 grams per hour of dry powder were used.

### TEST SPECIMENS

In rolling-contact fatigue testing, the contacting surfaces and the lubricating film each play an important role in determining the time to failure; together they constitute the specimen in any one test. A life distribution measuring the fatigue performance of one binary material-lubricant combination is valid only with reference to another binary combination. In each of the investigations described herein, a trend was established by holding one element constant and evaluating the other as the controlled variable or, in the case of controlled environmental variables, the test specimens were held constant. Properties of test specimens for the individual investigations are given in tables I and II.

### TABLE I.—ANALYSIS AND CLEANLINESS OF BALL SPECIMENS

| Specimens | ASTM cleanliness A– | ASTM cleanliness D– | Cleanliness sub-group | Analysis (specified), percent C | P (max.) | S (max.) | Mn | Si | Al | Cr | V | W | Mo |
|---|---|---|---|---|---|---|---|---|---|---|---|---|---|
| SAE 52100 (air-melt) | 1 | 1 | Poor | 1.00 | 0.025 | 0.025 | 0.35 | 0.28 | ---- | 1.45 | ---- | ----- | ---- |
| AISI M-1 (air-melt) | 1 | 1 | Fair | .80 | .030 | .030 | .23 | .23 | ---- | 4.00 | 1.00 | 1.50 | 8.00 |
| MHT (air-melt) | 1 | 1 | Poor | .98 | .025 | .025 | .40 | .54 | 1.25 | 1.38 | ---- | ----- | ---- |
| TMT (air-melt) | 1 | 1 | Poor | 1.00 | .025 | .025 | .50 | 1.00 | .08 | 1.45 | ---- | ----- | .30 |
| AISI M-10 (air-melt) | 1 | 1 | Poor | .85 | .030 | .030 | .23 | .30 | ---- | 4.00 | 2.00 | ----- | 8.00 |
| Halmo (vacuum-melt) | 1 | 1 | Good | .65 | .030 | .030 | .27 | 1.2 | ---- | 4.72 | .55 | ----- | 5.36 |
| AISI T-1 (air-melt) | 1 | 1 | Excellent | .70 | .030 | .030 | .30 | .25 | ---- | 4.00 | 1.00 | 18.00 | ---- |
| AISI MV-1 (air-melt) | 1 | 1 | Good | .80 | .030 | .030 | .30 | .25 | ---- | 4.10 | 1.10 | ----- | 4.25 |
| AISI M-50 (air-melt) | 1 | 1 | Good | .80 | .030 | .030 | .30 | .25 | ---- | 4.00 | 1.10 | ----- | 4.00 |
| AISI M-1 (vacuum-melt) | 1 | 1 | Excellent | .80 | .030 | .030 | .23 | .23 | ---- | 4.00 | 1.00 | 1.50 | 8.00 |

TABLE II.—LUBRICANT PROPERTIES

| Lubricant | Viscosity, centistokes | | | | | | Viscosity index | | | Neutralization number | | Pressure-viscosity coefficient, psi⁻¹ [b] |
| | Before | | After [a] | | Average | | Before | After | Average | Before | After [a] | |
| | 100° F | 210° F | 100° F | 210° F | 100° F | 210° F | | | | | | |
|---|---|---|---|---|---|---|---|---|---|---|---|---|
| SAE 10 | 44.0 | 6.4 | --- | --- | --- | --- | --- | --- | 104.0 | 0.05 | 0.05 | --- |
| MIL-O-6081B-2, grade 1005 | 5.07 | 1.68 | 5.13 | 1.72 | 5.10 | 1.70 | --- | --- | 104.5 | .05 | .05 | --- |
| MIL-O-6081B-2, grade 1010 | 10.14 | 2.49 | 10.37 | 2.54 | 10.26 | 2.52 | --- | --- | 73.2 | .05 | .05 | --- |
| MIL-L-15016A-2, grade 3042 | 24.20 | 4.51 | 24.26 | 4.57 | 24.23 | 4.54 | --- | --- | 114.0 | .05 | .05 | --- |
| MIL-L-6082B grade 1065 | 118.6 | 11.94 | 119.56 | 12.27 | 119.1 | 12.11 | --- | --- | 99.4 | .06 | .06 | --- |
| Methyl silicone | 10.27 | 4.42 | 10.34 | 4.43 | 10.31 | 4.42 | 270.0 | 270.0 | 270.0 | .05 | .05 | 8.35×10⁻⁵ |
| Paraffinic-base mineral oil | 10.14 | 2.49 | 10.37 | 2.54 | 10.26 | 2.52 | 70.5 | 74.3 | 72.4 | .05 | .05 | 5.38×10⁻⁵ |
| Water-soluble polyalkylene glycol | 8.62 | 2.27 | 8.75 | 2.28 | 8.69 | 2.28 | 75.7 | 72.7 | 74.2 | 1.03 | 1.05 | 3.28×10⁻⁵ |
| Di(2-ethylhexyl) sebacate (MIL-L-7808C) | 13.5 | 4.91 | --- | --- | --- | --- | 232.0 | --- | --- | --- | .15 | 2.52×10⁻⁵ |
| Diisooctyl adipate | 9.80 | 2.76 | 9.73 | 2.76 | 9.77 | 2.76 | 141.0 | 143.0 | 142.0 | 1.32 | 1.35 | Unavailable |

a Obtained from unused lubricants retained in storage and taken after test.
b Obtained from ref. 17 for lubricants similar to those used herein.

## BALLS

Predetermined axes of spin for ball specimens were established either by grinding flats at the extremities of the spin axis or by drilling a hole through the ball. This facilitated preinspection of the test surface and restarting of an unfailed ball on the same track.

## CYLINDERS

The nominal dimensions of the test cylinders are as follows: 4.750 inches outside diameter by 3.00 inches long, with an initial nominal inside diameter of 3.250 inches. The bore surface finish was 2 to 3 microinches for all cylinders. Roundness of the bore was held to 0.0001 inch and bore taper to 0.0003 inch maximum. Hardness measurements were taken on the cylinder ends. Each cylinder was uniform within two hardness numbers, although the average hardness for different cylinders varied between Rockwell C–60 and C–64.

A cylinder bore may be used for approximately 15 separate test tracks, and, by regrinding the bore 0.060 inch larger and refinishing the surface, the cylinder may be reused. This new surface is about 0.022 inch below the location of the maximum-shear-stress location of the previous tests; therefore, the effects of prior stressing are considered to be negligible. Analysis of the failure locations of the reground surface showed that these failure locations did not correlate with failure locations of the previous test surface.

## PROCEDURE

### PRETEST INSPECTION

Test balls were weighed and given a surface inspection at a magnification of 60. A record of surface conditions such as cracks, laminations, flat spots, and excessive scratches or pitting was maintained for post-test reference. Care was taken to secure high-quality balls, and no rejections were made during the pretest inspection in an effort to avoid biased results. During storage all specimens were coated with a corrosion-inhibiting oil.

Cylinders were given dimensional surface-finish and hardness inspections. This was followed by a magnetic particle inspection for cracks and large subsurface inclusions and a visual inspection for deep scratches and other mechanical damage.

## ASSEMBLY OF RIG

The rig and test specimen were cleaned and assembled with care to prevent scratching of the bore surface. The bore surface and test balls were coated with lubricant. The test position in the cylinder was set by loosening the collet (fig. 1), moving the nozzle assembly and the test balls axially to the test station, and then retightening the collet. The rig was mounted in the support frame and then leveled. Instrumentation was connected and adjusted.

### STARTING AND RUNNING PROCEDURE

The rig was brought up to operating speed as rapidly and smoothly as possible. Run-in, during which resistance to rolling decreased, was rapid during the first few minutes and was stabilized after the first hour. The stabilization time for test temperature was negligible (less than 3 min) for 100° F tests and was achieved with the 450° F tests in about 20 minutes.

Speed, temperature, and oil flow were monitored regularly. Speed, temperature, air pressure, and vibration levels were recorded at each reading. The test was continued until a predetermined number of stress cycles had been exceeded or until a ball or race failure actuated the meter relay that shut down the rig.
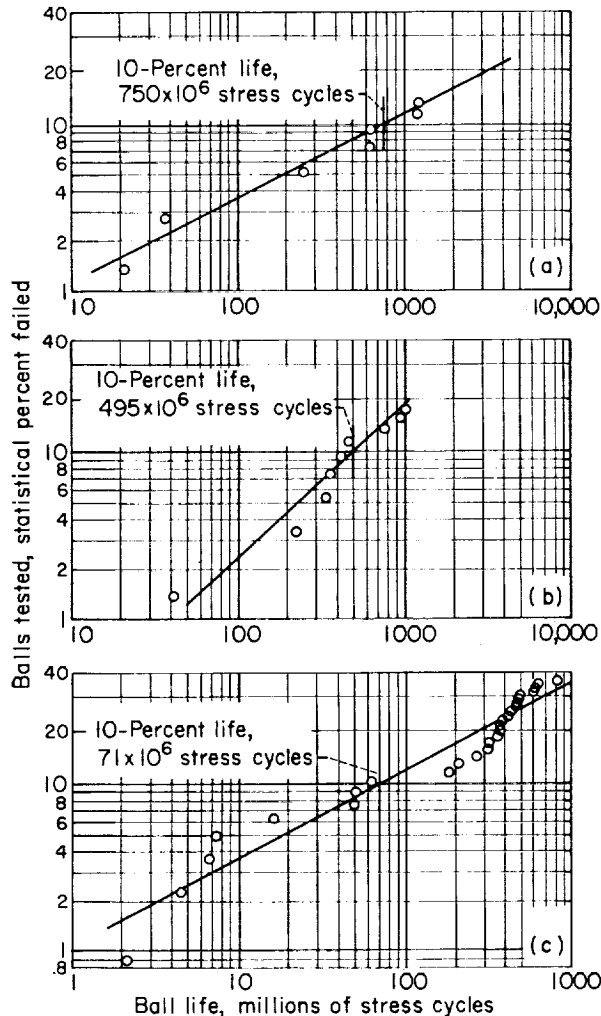
### STRESS CALCULATIONS

With ball weight, speed, and orbital radius of rotation known, the load can be calculated. The stress developed in the contact area was calculated from the load and specimen geometry by using the modified Hertz formulas given in reference 9.

### POST-TEST INSPECTION

After failure, or a predetermined number of stress cycles, the ball running tracks were examined with a microscope at a magnification of 60. Any abnormalities that correlated with the fatigue-life results were noted and were followed by a further metallographic investigation. Specimens were mounted in Bakelite, ground to the desired cross section, and polished and etched to reveal subsurface metallographic structure. Standard techniques were used for preparing metallographic specimens, but extreme care was taken during grinding to avoid overheating. Incremental sections across the running track were often taken in an effort to observe as much of the structure as possible.

## PRESENTATION OF LIFE DATA

Failure data were plotted on Weibull coordinates, which gave a plot of the log log of the reciprocal of the sample portion surviving against the log of the stress cycles to failure. Median ranks (ref. 10) were used as the survival coordinate for data points; a median rank is an estimate of the true rank in the population that has an equal probability of being too large or too small. Lines were fitted to these data points by the least-squares method.

## RESULTS AND DISCUSSION

### COMPARISON WITH FULL-SCALE BEARING TESTS

Groups of SAE 52100 test balls (table I) were run at room temperature on AISI M-50 (MV-1) and AISI M-1 test cylinders with an SAE 10 paraffinic mineral oil lubricant (table II). Results for the balls at 600,000-, 675,000-, and 750,000-psi maximum Hertz compressive stress are given as Weibull plots in figure 2. Results for the MV-1 race cylinders are given in figure 3. No



(a) Maximum Hertz stress, 600,000 psi; sample, 50 balls; 7 failures.

(b) Maximum Hertz stress, 675,000 psi; sample, 50 balls; 9 failures.

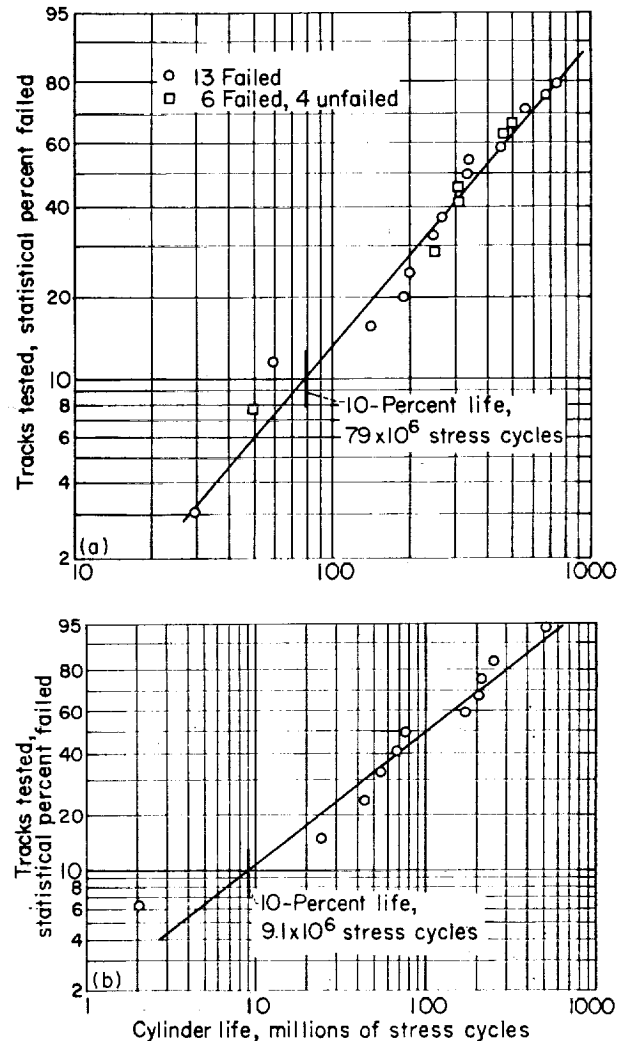(c) Maximum Hertz stress, 750,000 psi; sample, 74 balls; 27 failures.

FIGURE 2.—Life of 9/16-inch SAE 52100 grade-1 balls at room temperature. Lubrication, SAE 10 mineral oil at 5 milliliters per hour.

(a) Maximum Hertz stress, 600,000 psi; sample, 23 tracks (two cylinders); 19 failures.

(b) Maximum Hertz stress, 750,000 psi; sample, 11 tracks; 11 failures.

FIGURE 3.—Life of MV-1 tool-steel cylinders at room temperature. Lubrication, SAE 10 mineral oil at 5 milliliters per hour.

results are given for the M–1 cylinders because of the limited data secured. Since the early failures (10-percent life) were of primary interest and in order to avoid prohibitively long test times, all tests were suspended after a predetermined number ($10^9$) of stress cycles.

**Stress-life relation.**—The failure lives for the ball data of figure 2 are plotted as a function of stress in figure 4. The slope of this line is the stress-life exponent. A line drawn between the 10-percent lives for the two extreme stress levels gives an exponent (slope) of 10. The 10-percent life for the middle stress level is somewhat higher than this line, but a least-squares line through all the 10-percent lives results only in a shift in position and not in a significant change in slope. The overall value for the three stress levels of figure 4 is 10.4. This compares with the accepted value for full-scale bearings of 9 to 10 given in reference 7.

The failure lives for the race data of figure 3 are plotted as a function of stress in figure 5. No data are available for the intermediate stress level, but the low- and high-stress-level results are believed adequate to establish the slope of the stress-life line. This line has a stress-life exponent (slope) of 9.7.

**Failure type.**—Figure 6 includes representative photographs of a bearing race failure (tested conventionally) and ball failures (tested in the spin rig); the section views were taken parallel to the plane of the contact track. Macro-
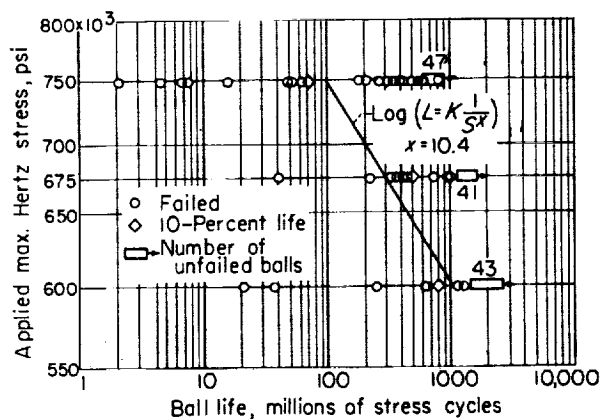


FIGURE 4.—Variation of ball life with applied stress. Balls, grade 1, %₁₆-inch SAE 52100 steel; room temperature; lubrication, SAE 10 mineral oil at 5 milliliters per hour.
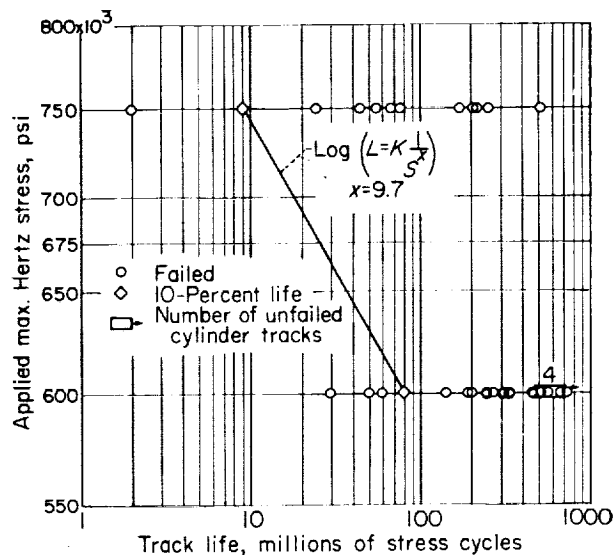


FIGURE 5.—Variation of track life with applied stress. Cylinders, MV–1 tool steel; room temperature; lubrication, SAE 10 mineral oil at 5 milliliters per hour.

photographs of a failed bearing race (size 222) and a ball failure obtained in the spin rig are shown in figures 6(a) and (d), respectively. The failures tend to cover the full width of the track.

The section views of figures 6(b) and (e) show that the spalling tends to be shallow in extent. Propagation cracks may be seen in both sections. The small inset (fig. 6(g)) illustrates the amount of detail that may be obtained from an early stage of ball test failure. The views of figures 6(c) and (f) show typical inclusion damage in the form of incipient cracking of the matrix. Such inclusion damage is more pronounced (in the number of inclusions affected and the extent of cracking) in the ball tests because of the higher stress concentration. Subsurface origin of failures has been observed for bearings (ref. 6) and for ball failures.

The fatigue failures obtained in the spin rig are of the same general type as observed in full-scale bearings. They are both characterized as being localized in nature and limited in depth of spalling and are usually of subsurface origin near the plane of maximum shear stress. This consistency of failure type and stress-life relation between the spin rig and full-scale bearing tests lends support to the fatigue spin rig as a valid test of factors governing fatigue life in rolling-contact bearings.

## FIBER ORIENTATION STUDIES

Any metallic object formed by forging generally possesses a fiber flow pattern that reflects the flow of metal during the forming operation. Since nonmetallic inclusions do not respond to the heat treatment used to control the metallographic structure of the material, they are progressively elongated during each forming operation from the ingot to the final bearing element shape in a manner that reflects the overall flow of the metal. This pattern is best described as fibrous in appearance, hence the term "fiber flow lines." Most materials have less static strength in a transverse (to fiber) direction, and sometimes the same effect is observed in fatigue properties (ref. 11). Steel balls as manufactured for bearings are formed by upsetting slugs of rod stock between hemispherical dies. The two areas (poles) corresponding to the ends of the rod slug receive less working, which results in a concentration of fibers and nonmetallics perpendicular to the surface area (fig. 7). A second region (equator) corresponding to the die parting line has perpendicular fiber due to the removed flashing. Bearing races can have one of several characteristic fiber patterns corresponding to the method of manufacture.

**Preliminary observations.**—Two groups of SAE 52100 test balls, one with predetermined tracks across the poles and one with tracks at 90° to the poles (i.e., on the equator), were run at room temperature with a mineral oil lubricant. All but one of the 13 balls run across the poles failed in the polar area (perpendicular fiber), although only 42 percent of the track was within the polar area. Of the 21 balls run on the equator, 16 survived the number of stress cycles at which all the polar
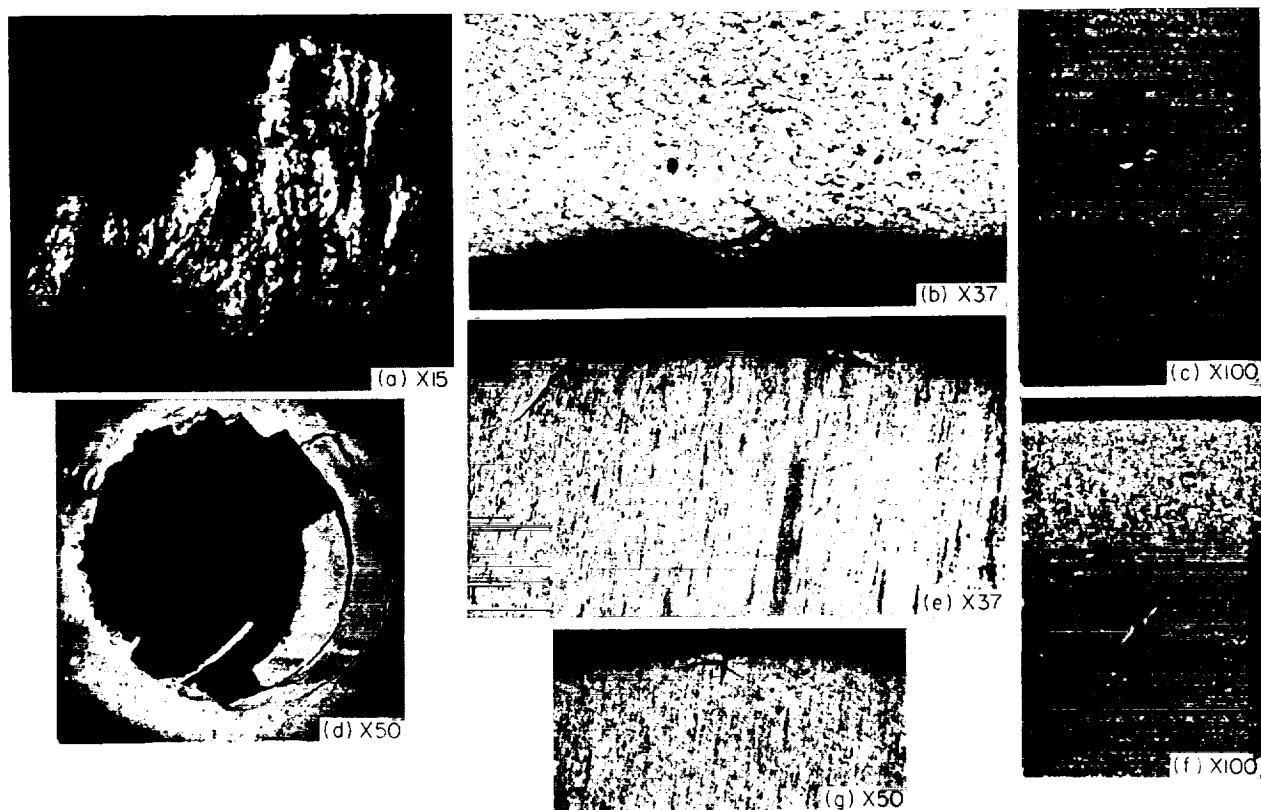


(a) Small spall on inner race of M-1 (222) bearing.
(b) Section view of part of same spall.
(c) Incipient failure near point of maximum shear stress.
(d) Typical spall, spin-rig-tested ball.
(e) Section view of spall.
(f) Incipient failure near point of maximum shear stress.
(g) Section view of early failure on spin-rig-tested ball.

FIGURE 6.—Comparison of failures of a bearing inner race and balls tested in rolling-contact fatigue spin rig.
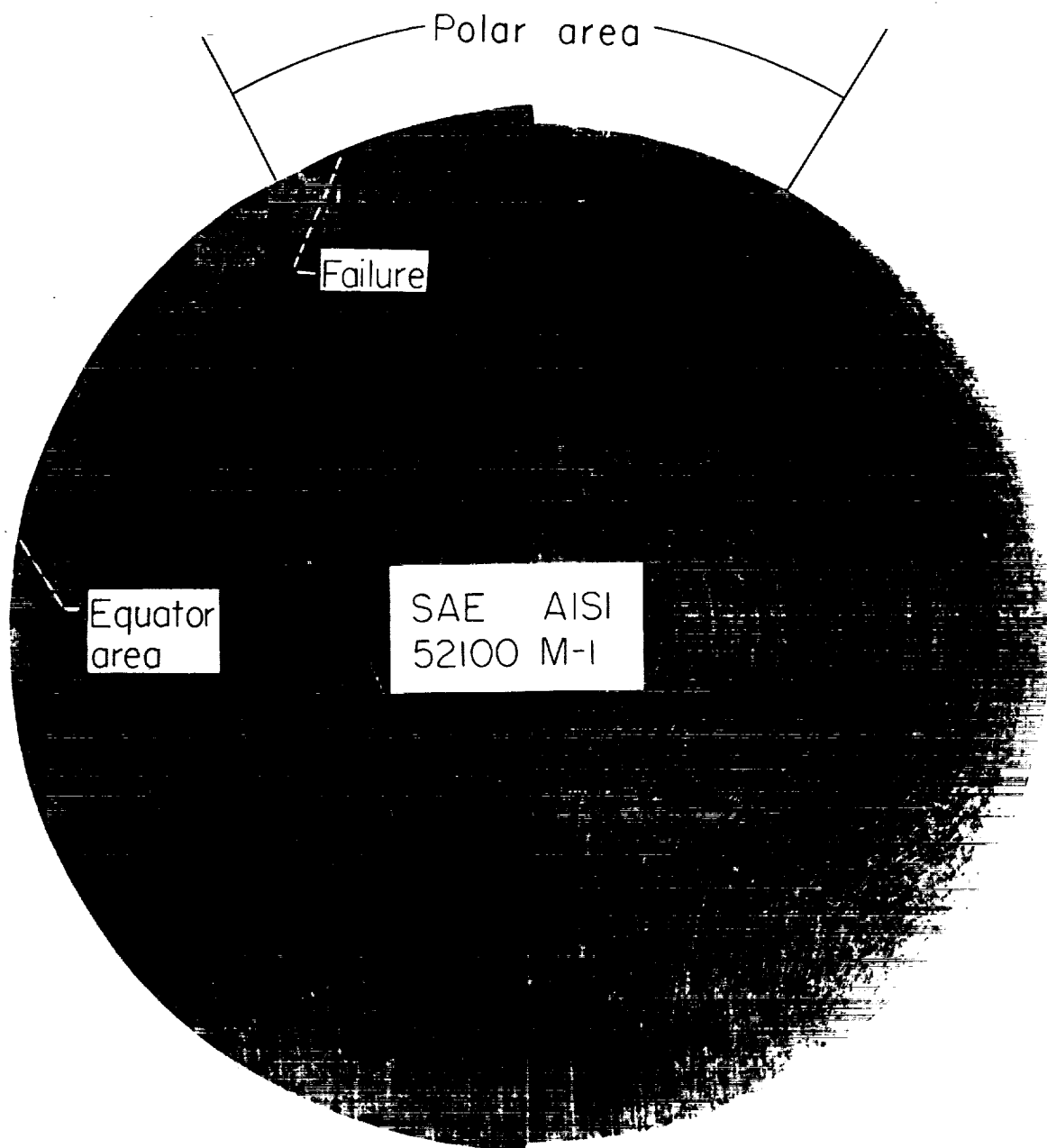
FIGURE 7.—Fiber orientation on SAE 52100 and AISI M–1 balls.

track balls had failed (fig. 8). These results indicated that a definite weakness of the polar area relative to the nonpolar area exists with respect to both life and density of failures.

A typical early failure stage in the polar area of concentrated perpendicular fiber is shown in figure 9. Chemical segregation (fiber) is parallel to the high compressive stress. Such structural inhomogeneity can result in changes of elastic modulus or act as a metallurgical stress raiser. It is believed that secondary tensile stresses normal to the fiber were too high and caused the fatigue crack indicated by A in figure 9. Shear cracks progressing from the original fatigue crack are shown by B. If the test were continued, these



(a) Across poles.
(b) On equator.

FIGURE 8.—Comparison of fatigue life for tracks on equator and across poles. SAE 52100 ½-inch balls; maximum Hertz stress, 714,000 psi; room temperature; synthetic sebacate lubricant.

would progress to open the characteristic shallow spall failure.

**Studies with controlled fiber orientation.**—Special test cylinders were machined from AISI T-1 (table I) billet stock with the bore axes oriented at 0°, 45°, and 90° to the billet axis. The first orientation gave a control cylinder with all fibers parallel to the bore surface. The latter two had a fiber pattern that produced a continuous range of controlled fiber orientation angle relative to the test surface of 0° to 45° and 0° to 90°, respectively, repeating in each quadrant of the running track. Tests were run at 750,000-psi maximum Hertz compressive stress with SAE 52100 ⁹⁄₁₆-inch balls and SAE 10 mineral oil at room temperature. Three surfaces, each containing about 20 test tracks, were run on each of the three test cylinders.

**Failure density.**—Failure location was correlated with fiber orientation angle by dividing the test surface into zones of equal area containing a portion of the total fiber orientation range and by counting the number of failures in each zone. This procedure produced the histograms shown in figure 10. The 0° control cylinder had a consistent fiber orientation parallel to the surface, and a random failure pattern was observed. The 45° cylinder (0° to 45° fiber-angle range) showed a definite trend (fig. 10(a)) toward a concentration of failures in the areas of highest fiber angle relative to the test surface. This contrast was even greater in the 90° cylinder (0° to 90° range), where the zone of highest fiber orientation angle had approximately triple the failure density of the zone of lowest fiber orientation angle (fig. 10(b)). Thus, there is a strong tendency for failures to concentrate in that part of the running track with fibers intercepting the test surface at angles approaching the perpendicular.

**Fatigue life.**—A greater than average failure density is an indication that an area is weak in fatigue strength. Thus, the running time (i.e., stress cycles) to failure should be shorter for the region where failure density is the greatest. Weibull plots for the life data in each of the five 18° zones from the 90° cylinder used to plot failure density in figure 10(b) are given in figure 11. To maintain statistical validity, failures in the other zones are considered suspended tests and are evaluated by the method of reference 12. This series of Weibull plots shows a continuous trend toward shorter failure life with increased fiber
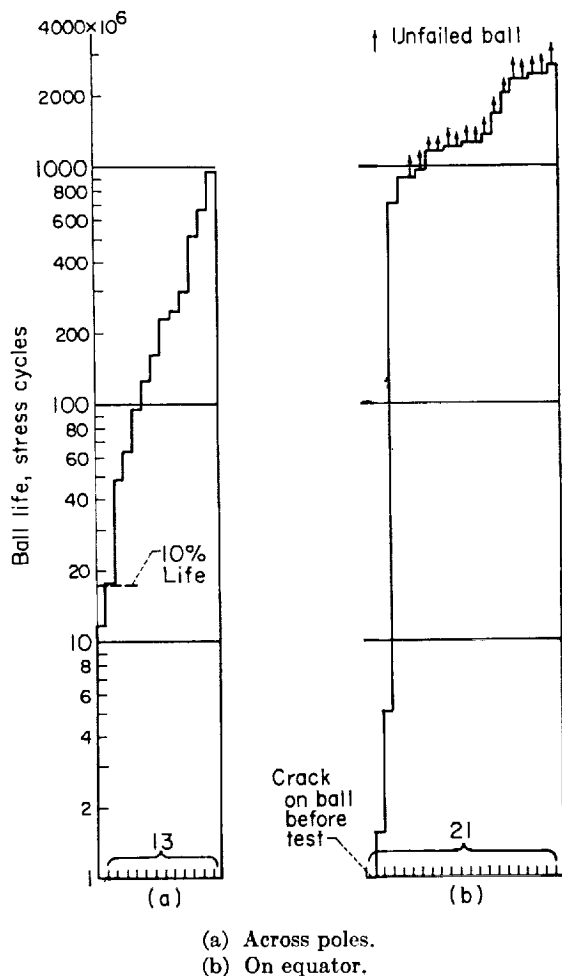
FIGURE 9.—Typical early failure stage in polar area.   SAE 52100; X100.

orientation angle. A plot of 10-percent life against fiber orientation angle (fig. 12) shows a consistent relation between life and fiber orientation. Perpendicular fibers produce only about one-fourth to one-fifth the life observed with parallel fibers. This life relation, together with the failure-density relation, is strong evidence that better rolling-contact fatigue performance can be anticipated for bearing elements fabricated with methods that avoid forging fibers intercepting the rolling surface.

Since the regions of high fiber angle contained material from the billet center where chemical segregation and inclusions tend to concentrate, while the regions of low fiber angle did not, the central part of the 0° to 90° cylinder containing the billet core was compared with the cylinder as a whole in order to evaluate the effect of distance from the billet axis (ref. 13). The central part of the test cylinder showed no significant deviation in fatigue life from that observed for the cylinder as a whole. A similar comparison of failure density
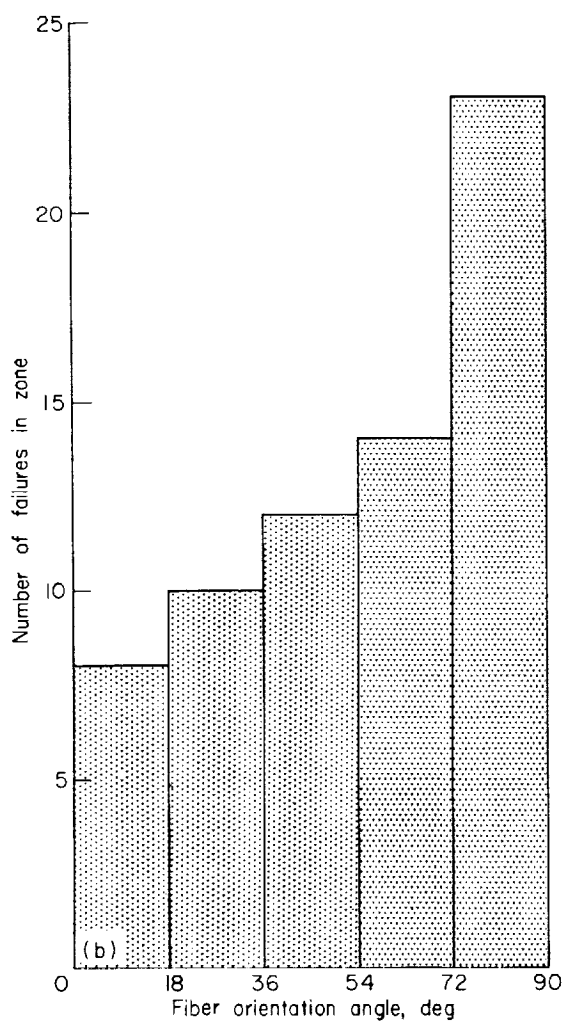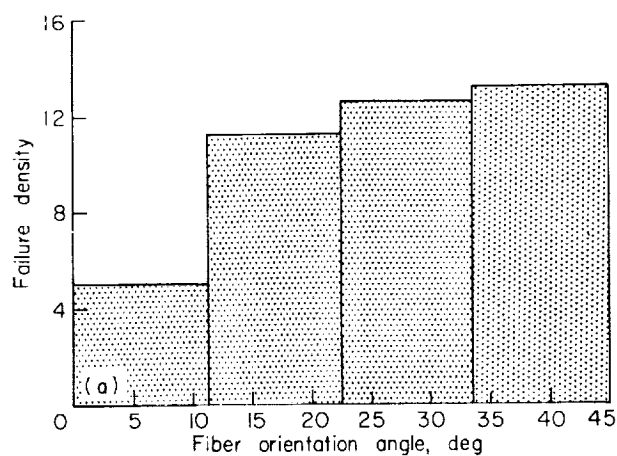
(a) 0° to 45° cylinder.
(b) 0° to 90° cylinder.

FIGURE 10.—Distribution of failures in test cylinders.
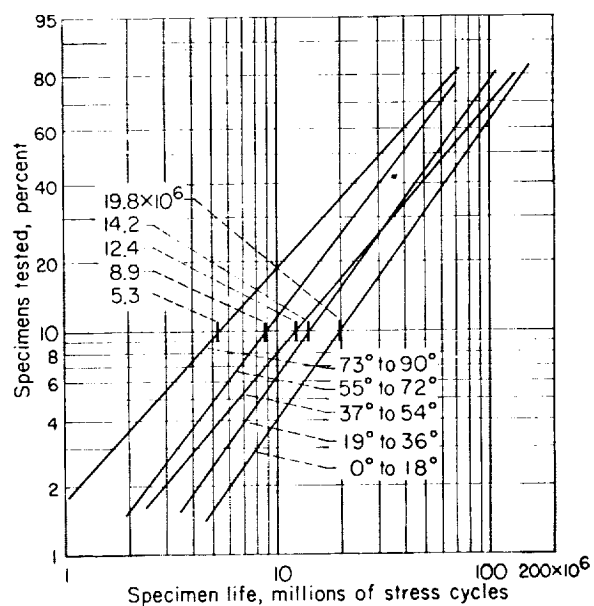


FIGURE 11.—Fatigue lives for five ranges of fiber orientation angle. Material, AISI T–1 tool steel; lubricant, SAE 10 mineral oil; maximum Hertz compressive stress, 750,000 psi; room temperature.
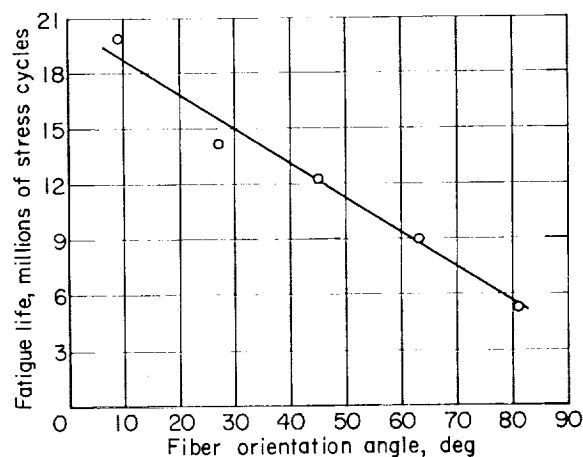


FIGURE 12.—Ten-percent failure life as function of average fiber orientation angle. AISI T–1 tool steel; room temperature; SAE 10 mineral oil; maximum Hertz compressive stress, 750,000 psi.

also showed that the effect of fiber orientation angle was more important than distance from the billet axis (ref. 13).

**Ball fiber pattern studies.**—A large group of balls, of which 211 failed, was tested with randomly oriented tracks and was used to obtain data on failure location with respect to fiber orientation. The large sample size assured random orientation. Post-test etching showed that about 63 percent of the tracks (in both the failed and unfailed balls) ran through the poles; this is in good agreement with the 64-percent theoretical value. This sample group consisted of subgroups of ten different materials.

Since the tracks of the balls were randomly oriented with respect to fiber orientation, a random failure pattern should have been produced if the balls were of uniform fatigue strength over the entire surface area. The probability of failure occurring in a polar area under various limiting conditions was computed in a previous report on fiber orientation effects on ball failures.

Experimental results for the entire sample of 211 balls (table III) showed a substantial increase in the number of failures occurring in the poles, compared with the theoretical results for a sphere of uniform fatigue strength. For the entire sample, the failures occurring in the poles (30.8 percent) are about twice the theoretically anticipated results. This disparity was observed for each of the material subgroups.

Experimental results for the 144 balls out of the total sample that had part of the running track within the poles (i.e., those that could produce either an intra- or extra-polar failure) also show a strong affinity for preferential failure in the polar area of high fiber-intersection angle (table III). For all 144 balls the portion of the failures occurring within the poles (45.1 percent) is about twice the theoretically anticipated concentration. Each of the ten material subgroups showed a similar tendency, indicating that the effect is independent of alloy content.

Figure 13 is a plot of failure density on the ball surface as a function of the elevation from the equator toward the pole (i.e., ball latitude). This figure was compiled from the failure position data obtained from the 211 balls examined. The data were plotted by counting all the failures in each of

nine 10° zones of ball latitude and dividing by a factor equal to the percentage of the total ball area in the zone; this gave a failure density for each zone. This plot shows a very marked increase in density of failures in the polar areas (higher ball latitude) where the fiber orientation is approximately perpendicular to the surface. The area near the equator also has a significant increase in failure density; this area has fiber orientation approaching perpendicular because of the removal of flashing formed at the upsetting die parting line. These characteristic fiber orientation areas are illustrated in figure 7. A plot such as figure 13 for a homogeneous material would present a uniform band of failure density.

A significant portion of the fatigue failures occurring outside the poles and equator also exhibited a unique appearance that apparently ties in with the fiber flow pattern originating in the upset forging of the balls. In this area, the fiber orientation is parallel to the surface, but open discontinuities perpendicular to the equator (die parting line) are frequently observed during pretest inspection at high magnification. Any such defects near the surface would cause stress concentrations and accelerate fatigue failure. Figure 14 shows this condition for one ball each of AISI M-10, AISI M-1, AISI T-1, and SAE 52100. In each case the failure occurred at a discontinuity that was at an angle to the running track but perpendicular to the equator. This condition was observed in approximately 30 percent of the balls that failed outside the poles. No correlation with the angle of track and discontinuity intersection was found. In most cases the discontinuity was observed in the preinspection and post inspection. The photographs in figure 14 were taken after etching.

All of these forging fiber orientation studies indicate that regions where the fiber direction approaches the normal to the rolling-contact surfaces have a much greater propensity for failure and shorter fatigue life than regions in the same specimen where the fiber is parallel to the surface. Substantial improvement in bearing life can be expected if a fabrication technique that minimizes this adverse condition at the rolling-contact surfaces of bearing elements is adopted.

TABLE III.—EXPERIMENTAL AND THEORETICAL FAILURE-LOCATION DISTRIBUTIONS IN RANDOMLY ORIENTED BALLS

| Material | Location of failures | Total sample | | | | Balls that ran over polar areas | | | |
|---|---|---|---|---|---|---|---|---|---|
| | | Experimental results | | Theoretical fraction of failures (a) | Ratio of experimental to theoretical results | Experimental results | | Theoretical fraction of failures (a) | Ratio of experimental to theoretical results |
| | | Number of failures | Fraction of failures | | | Number of failures | Fraction of failures | | |
| SAE 52100, 9/16" diam. | Polar area | 14 | 0.326 | 0.15 | 2.17 | 14 | 0.560 | 0.234 | 2.39 |
| | Nonpolar | 29 | .674 | .85 | .79 | 11 | .440 | .766 | .57 |
| AISI M-1, 1/2" diam. | Polar area | 15 | .205 | .15 | 1.37 | 15 | .300 | .234 | 1.28 |
| | Nonpolar | 58 | .795 | .85 | .94 | 35 | .700 | .766 | .97 |
| AISI M-1 (vacuum-melt), 1/2" diam. | Polar area | 3 | .231 | .15 | 1.54 | 3 | .375 | .234 | 1.60 |
| | Nonpolar | 10 | .769 | .85 | .90 | 5 | .625 | .766 | .82 |
| AISI MV-1, 1/2" diam. | Polar area | 5 | .217 | .15 | 1.45 | 5 | .385 | .234 | 1.65 |
| | Nonpolar | 18 | .783 | .85 | .92 | 8 | .615 | .766 | .80 |
| AISI M-10, 1/2" diam. | Polar area | 4 | .444 | .15 | (b) | 4 | .572 | .234 | 2.44 |
| | Nonpolar | 5 | .556 | .85 | --- | 3 | .428 | .766 | .56 |
| AISI M-50, 1/2" diam. | Polar area | 5 | .417 | .15 | (b) | 5 | .556 | .234 | 2.37 |
| | Nonpolar | 7 | .583 | .85 | --- | 4 | .444 | .766 | .58 |
| MHT, 1/2" diam. | Polar area | 2 | .167 | .15 | 1.11 | 2 | .286 | .234 | 1.22 |
| | Nonpolar | 10 | .833 | .85 | .98 | 5 | .714 | .766 | .93 |
| TMT, 1/2" diam. | Polar area | 10 | .833 | .15 | (b) | 10 | .833 | .234 | 3.56 |
| | Nonpolar | 2 | .167 | .85 | --- | 2 | .167 | .766 | .22 |
| Halmo, 1/2" diam. | Polar area | 5 | .500 | .15 | (b) | 5 | .500 | .234 | 2.14 |
| | Nonpolar | 5 | .500 | .85 | --- | 5 | .500 | .766 | .65 |
| AISI T-1, 1/2" diam. | Polar area | 2 | .500 | .15 | (b) | 2 | .667 | .234 | 2.85 |
| | Nonpolar | 2 | .500 | .85 | --- | 1 | .333 | .766 | .44 |
| Total | Polar area | 65 | .308 | .15 | 2.05 | 65 | .451 | .234 | 1.93 |
| | Nonpolar | 146 | .692 | .85 | .81 | 79 | .549 | .766 | .72 |

a For a homogeneous material.
b Computations omitted because track orientation in subgroup was not approximately random.

Polar area

90°

80°

70°

60°

50°

40°

30°

20°

10°

Failure
density

Fiber flow
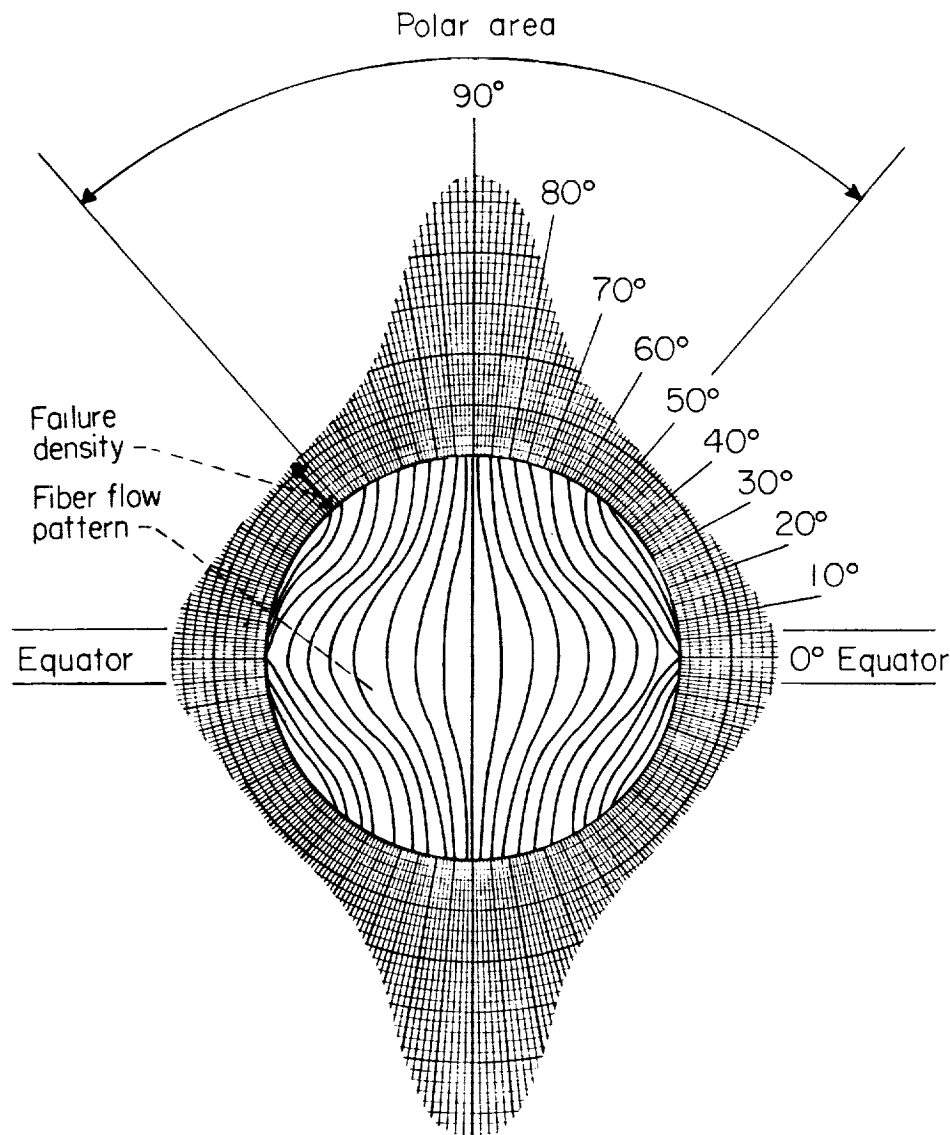pattern

Equator

0° Equator

FIGURE 13.—Failure density as function of ball latitude
(for 211 failures and 10 materials).

### LUBRICANT VISCOSITY

Most rolling-contact bearings operate in a viscous fluid that, in addition to lubrication and cooling, produces a continuous film in the contact zone. This film is subjected to the contact pressure and, during the short period of contact by a given surface area, actually sustains the bearing load. Since the ability of this film to carry the high loading is dependent on its resistance to flow away from the contact zone (viscosity) within the short period of loading, lubricant viscosity should

have a significant effect on rolling-contact fatigue life.

The literature available on the role of the lubricant in rolling-contact fatigue is limited. In references 4 and 14, the test temperatures are varied to vary the viscosity. Metallurgical transformation in the materials may be significant within the temperature range necessary to produce an adequate viscosity range (ref. 15). Any chemical reactions at the contact surface and in the lubricant would be influenced by temperature.

(a) AISI M-10.
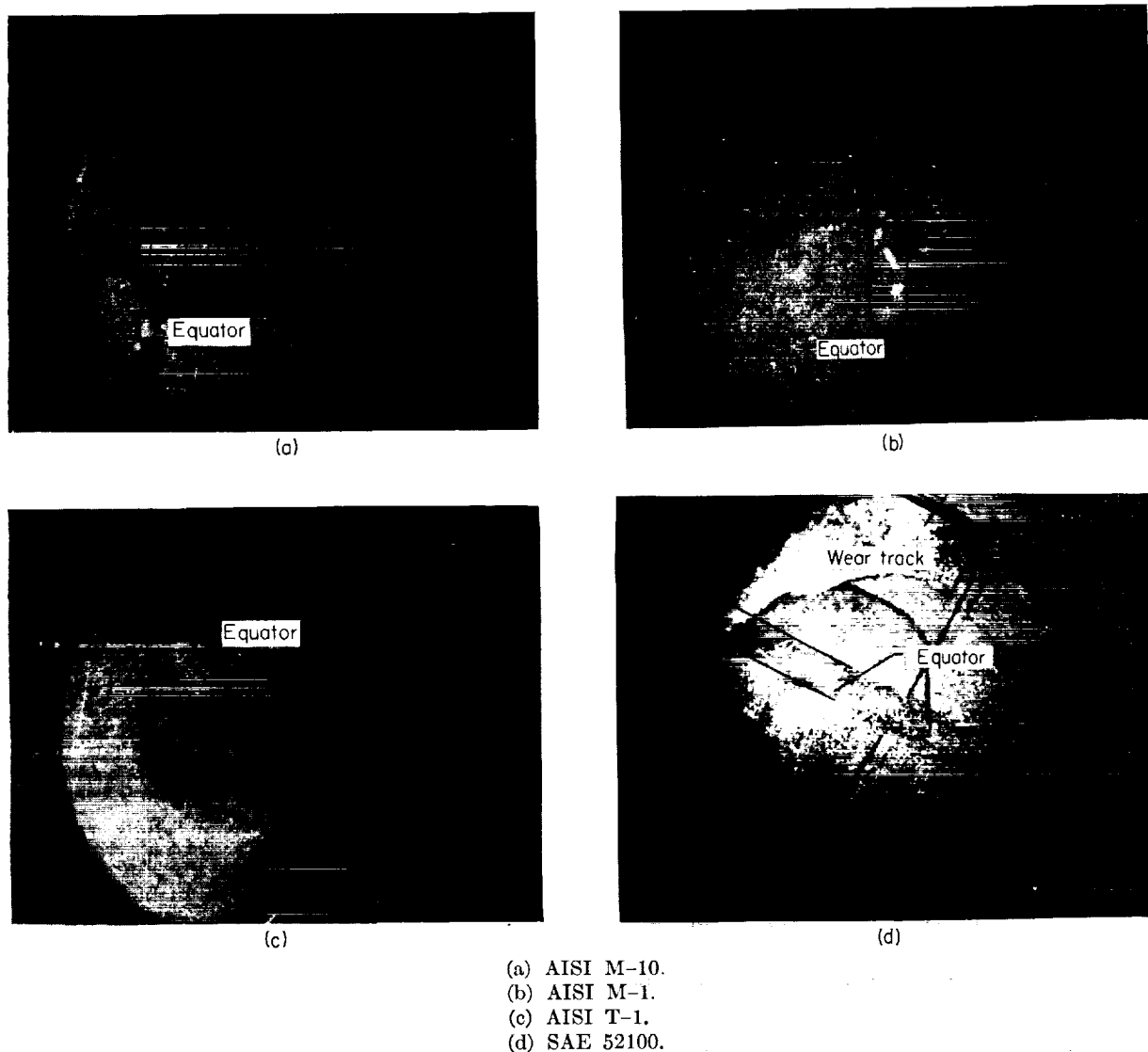(b) AISI M-1.
(c) AISI T-1.
(d) SAE 52100.

FIGURE 14.—Typical failure-causing discontinuities perpendicular to equator and coincident with failure fault line.

Reference 16 shows a linear increase in life with lubricant viscosity. Though not stated, it appears that the lubricants are all paraffinic-base stocks and that the tests were conducted at room temperature. This is a more controlled evaluation of the effect of lubricant viscosity on rolling-contact fatigue life, although the low scatter in life (2:1 or less) is not characteristic of bearing-fatigue data and may indicate overloading and crushing of the balls.

Another possible method of varying viscosity is to use lubricants of different base stock. This also introduces variables other than normal (atmospheric-pressure) viscosity, such as pressure-

viscosity effects and chemical reactions in the lubricant. Normal viscosity is that viscosity which is measured by standard tests at atmospheric pressure. Viscosity tends to increase significantly at the high pressure existing in bearing lubricating films (ref. 17). This effect is of varying degree in various base stocks. For this reason different base stocks may have different effects on fatigue life, even though the measured (normal) viscosity is constant.

The best method of observing the effects of lubricant viscosity on rolling-contact fatigue life would be the use of a series of fluids of the same base stock (i.e., same temperature and pressure-

viscosity characteristics) but with a range of viscosity as measured at atmospheric pressure. All other test conditions could then remain constant. The controlled variable would thus be the normal lubricant viscosity.

**Results.**—Four common paraffinic-base mineral oils with normal (atmospheric pressure) viscosities ranging from 5 to 119 centistokes at 100° F were used; other test conditions were held constant. AISI M–1 tool-steel balls were run at 100° F, at a load producing 725,000-psi maximum Hertz compressive stress and 225,000-psi maximum shear stress 0.009 inch below the running track. Material properties are summarized in table I, and lubricants in table II. Weibull plots for tests with the four oils having viscosities of 5.1, 10.3, 24.2, and 119.1, respectively, are given in figure 15. A summary of these results is given in the following table:

| Kinematic viscosity, centistokes | Sample size | Failures | Runouts | 10-Percent failure life, stress cycles | 50-Percent failure life, stress cycles |
|---|---|---|---|---|---|
| 5.1 | 18 | 15 | 3 | $16.7 \times 10^6$ | $335 \times 10^6$ |
| 10.3 | 17 | 13 | 4 | 20 | 350 |
| 24.2 | 19 | 14 | 5 | 23 | 410 |
| 119.1 | 15 | 15 | 0 | 36 | 550 |

The Weibull plots all have the same general appearance, but they shift toward the right (increased life) while the slopes (scatter) remain about the same. Thus, the shift toward longer life with
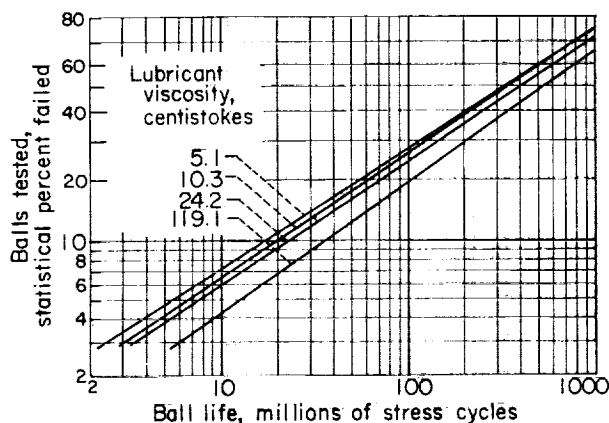


FIGURE 15.—Rolling-contact fatigue life of AISI M–1 tool-steel balls with paraffinic mineral oils. Test temperature, 100° F; maximum Hertz compressive stress, 725,000 psi.

increased lubricant viscosity exists at all survival levels (portion of total sample failed).

Other manifestations of rolling-contact stressing such as failure appearance and origin, metallurgical transformation in subsurface shear zone, and chemical activity on the test surface appeared to be consistent for all four tests.

**Discussion.**—Since there is a continuous trend toward longer rolling-contact fatigue life with increased lubricant viscosity within the range studied (5 to 120 centistokes), it is possible to plot a curve for this relation. Figure 16 is a plot of the log of fatigue life (10% and 50% failures) against the log of viscosity. This plot is almost linear; straight lines have been drawn for 10- and 50-percent failures by the least-squares method. These lines resolve with the following relation:

$$L = K\eta^N$$

where $L$ is fatigue life in millions of stress cycles and $\eta$ is lubricant viscosity in centistokes at 100° F. Then,

$$10\% \text{ fatigue life} = 11.3\eta^{0.237}$$

$$50\% \text{ fatigue life} = 245\eta^{0.167}$$

These relations indicate that the rolling-contact fatigue life is a function of about the 0.2 power of lubricant viscosity, which contrasts with the results of references 4, 14, and 16 where the life is given a linear relation to viscosity; although in all cases the rate of change of life with viscosity is about the same over the 5- to 119-centistoke range.

A more complex but more versatile equation can be fitted to the results for life against lubricant viscosity by a consideration of extreme-value theory. Since each failure results from the weakest point on the running track, all other points on the track are of necessity stronger; thus, the fatigue lives observed are a series of extreme values for all the infinitesimal areas of the running tracks. An extreme-value analysis results in an equation of the form

$$Q = e^{-\left(\frac{L \times 10^{-1}}{5 + 0.42\sqrt{\eta}}\right)^{(0.625 + 0.007\sqrt{\eta})}}$$

where $Q$ is the probability of survival and $L$ is the life in millions of stress cycles. In this form the relation can be used to calculate the life as a function of viscosity at any level of survival. This
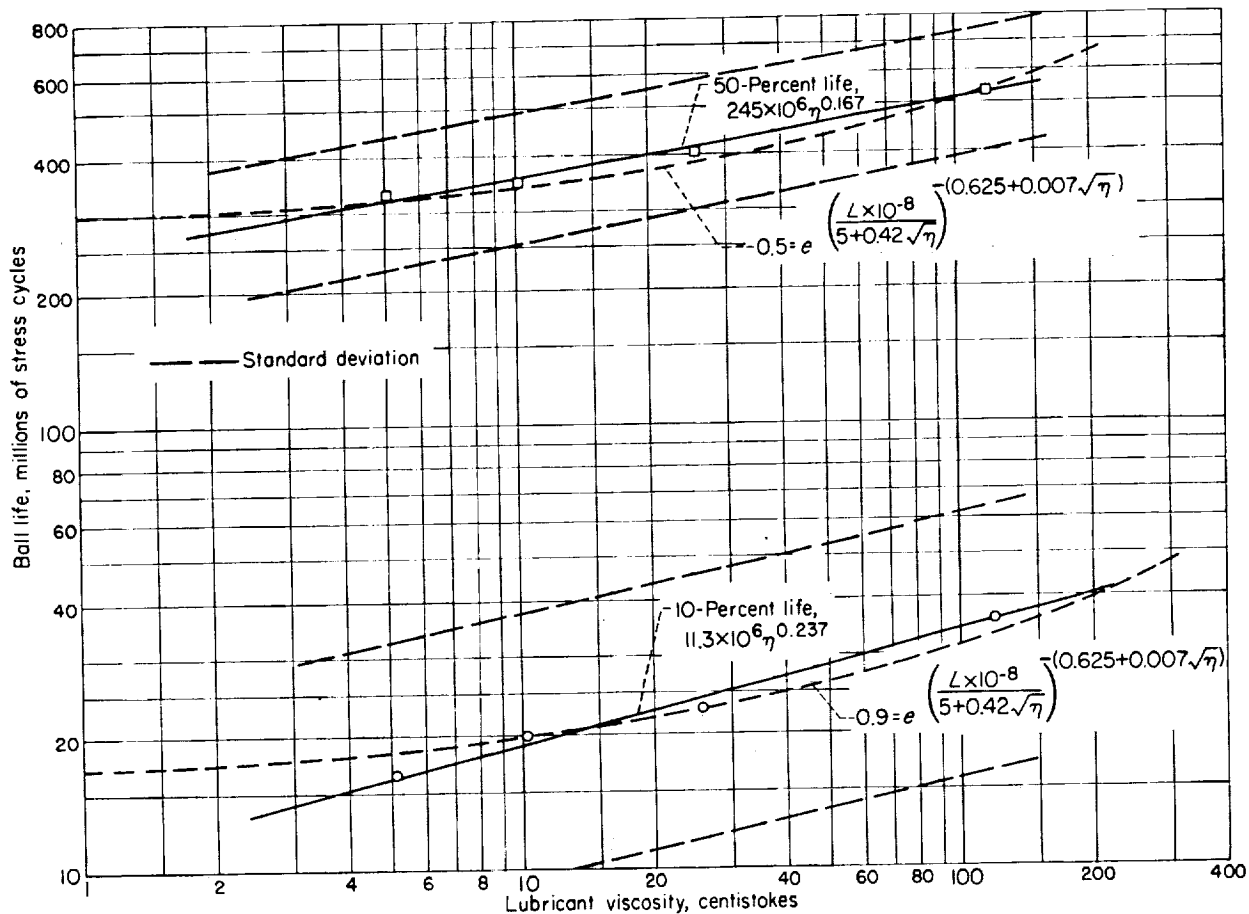
FIGURE 16.—Variation of ball life with lubricant viscosity. Test temperature, 100° F; maximum Hertz compressive stress, 725,000 psi.

curve is plotted for 10- and 50-percent lives in figure 16. This form would, upon extrapolation, give a finite fatigue life at zero viscosity, where the simple power function would not. For this reason it is considered to be a more reasonable form of the life-viscosity function, although a greater range of viscosity would be needed to establish it accurately at the low viscosity levels.

As with any measurement, the confidence in this data is limited by its statistical reliability. With rolling-contact fatigue data, the wide scatter normally encountered necessitates large sample sizes in order to establish accurately the relation of life against percent survival in the Weibull plot. At the same time, the expense and duration of each test limit the practical number of specimens that can be evaluated. Confidence limits for the data in figure 15 were calculated by the method of Lieblein (ref. 18) and are presented in figure 16. For the sample sizes of 15, 17, 18, and 19 balls

used to produce figure 15, these confidence limits are wide in relation to the range observed among the results for the different viscosity fluids. However, if no effect due to lubricant viscosity exists, the probability that the four life plots will fall in order of ascending viscosity is only 1 in 24. This is so because each of the lines was calculated by a least-squares best-fit technique so that these lines are objective. Thus, the results in figure 16 have a 96-percent probability not to have been caused by chance.

The preceding results indicate that the physical properties of the surrounding fluid can have a significant effect on rolling-contact fatigue life. It is of interest to consider how a fluid substance can remain in the highly pressurized contact zone where the failures causing stresses are produced, when it is free to flow away from it. This apparent anomaly is dependent on the relative motion of the contacting surfaces and the fluid between them.

During high-speed rolling contact, the lubricant, in addition to reducing sliding friction and cooling the bearing, affects the pressure distribution in the contact zone through hydrodynamic action. The theoretical calculations of stress are for static loading only. At high rolling speeds these may not be entirely correct. A precise three-dimensional analysis of this phenomenon would be very complicated, but a general discussion will illustrate the point.

Figure 17(a) is a cross section of the contact zone and pressure distribution for a ball running without a lubricant. The integral of pressure across the contact zone would be the total ball loading; thus, for a given load, the maximum pressure (i.e., compressive stress borne by the ball) would depend on the size of the contact area. Figure 17(b) shows how the presence of a lubricant might extend the effective load-carrying area and thus reduce the maximum pressure. The lubricant film ahead of the ball must be reduced to the minimum film thickness in the contact zone. For a given speed this requires a proportional rate of shear in the lubricant ahead of the ball to remove the excess fluid from the ball path. The force necessary to maintain this rate of shear depends on the viscosity of the fluid. Thus, a more viscous

fluid would require a greater shear force. Since this shear force is resolved from the pressure between the adjacent rolling-element surfaces, a portion of the ball load is borne by that part of the fluid outside of the contact area that would exist if no lubricant were present. Thus, the effective contact area is increased and the maximum contact pressure is reduced. For a given rolling speed, the maximum contact pressure would decrease with increasing lubricant viscosity. Since life is inversely proportional to the tenth power of maximum stress, the effect of lubricant viscosity in high-speed rolling contact could be significant. A two-dimensional mathematical analysis of this effect is given in reference 19.

### LUBRICANT BASE STOCK

The effect of lubricant viscosity on fatigue life observed in the preceding investigation is a correlation of life with the viscosity measured at atmospheric pressure. At a constant temperature, viscosity is known to increase substantially with pressure (ref. 17). This increase is a function of the atmospheric viscosity and the base stock of the lubricant. Since the lubricating fluid in the contact zone of the rolling elements is under very high pressure, the actual viscosity in the contact zone would be much higher than the viscosity at atmospheric pressure. In fluids of the same base stock, the actual viscosity is approximately proportional to atmospheric viscosity. However, viscosities of fluids of different base stock increase at different rates with pressure, so dissimilar fluids having the same atmospheric viscosity should produce different fatigue-life results.

Results.—Tests on AISI M-1 tool-steel balls (table I) were run with a methyl silicone, a paraffinic mineral oil, a glycol, a sebacate, and an adipate lubricating fluid to evaluate the effect of base stock. Properties of these fluids are given in table II. Each fluid had an atmospheric-pressure kinematic viscosity of approximately 10 centistokes at the 100° F test temperature.

Weibull plots for the fatigue lives with these fluids at 725,000-psi maximum theoretical Hertz compressive stress and 225,000-psi maximum shear stress 0.009 inch below the test surface are given in figure 18. These results are summarized in the following table.
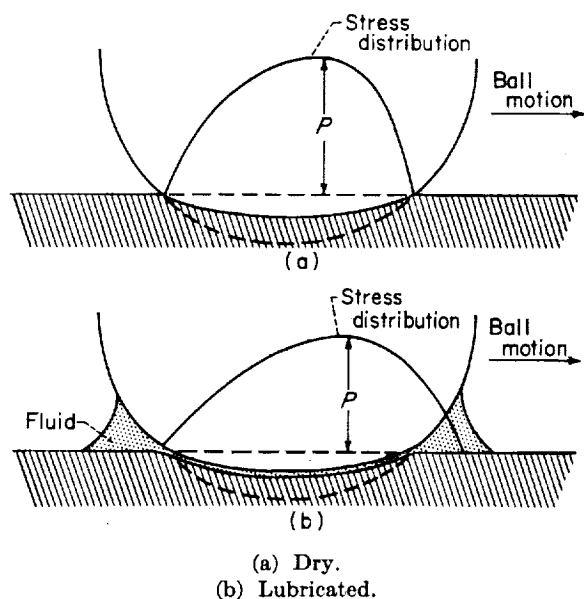


(a) Dry.
(b) Lubricated.

FIGURE 17.—Longitudinal section diagram of stress distribution in a rolling sphere.

| Lubricant | Pressure-viscosity coefficient, psi$^{-1}$ | Sample size | Failures | Runouts | 10-Percent failure life, stress cycles | 50-Percent failure life, stress cycles |
|---|---|---|---|---|---|---|
| Methyl silicone | 8. 35×10$^{-5}$ | 26 | 5 | 21 | 106×10$^6$ | ᵃ17, 000×10$^6$ |
| Paraffinic mineral oil | 5. 38 | 28 | 14 | 14 | 18 | 660 |
| Glycol | 3. 28 | 16 | 11 | 5 | 7. 6 | 167 |
| Sebacate | 2. 52 | 22 | 15 | 7 | 5. 2 | 200 |
| Adipate | Unavailable | 26 | 12 | 14 | 2. 4 | 1, 000 |

ᵃ Extrapolated.

The number of failed balls in the silicone group is fewer than that usually considered desirable for an evaluation of a lubricant-material combination. However, extremely long life was observed with this lubricant. This life was superior to that observed with the other lubricants studied. A greater number of failures would have entailed multiplying already excessive test run times. Even though only a limited number of failures was obtained, the Weibull plot for those points was close to a straight line. In view of this and the large number of balls tested without failure after more than one billion stress cycles, the data are considered conclusive to the extent that the methyl silicone is a superior lubricant in rolling-contact fatigue under these test conditions.

**Discussion.**—The wide range in life results with the five lubricants is readily apparent from the preceding table and from figure 18. These results as measured by the 10-percent failure lives show a range of approximately 40 to 1 between the silicone (longest life) and the adipate (shortest life). Since all test conditions were held constant except for the lubricating fluids, the action of the lubricant must play an important role in fatigue life.

The small variations in normal viscosity, as measured at atmospheric pressure (8.75 to 13.5 centistokes, 8.7 to 11.8 centipoises), of the fluids used (table II) would account for a life range of only about 1.05 to 1 based on the life-viscosity relation of figure 16. This range can be considered negligible when compared with the observed range (fig. 18) obtained with fluids of different base stock.

Another possible cause of variation in fatigue life from one lubricant to another could be the variation in type and intensity of chemical action at the contacting surfaces. Since the five lubri-
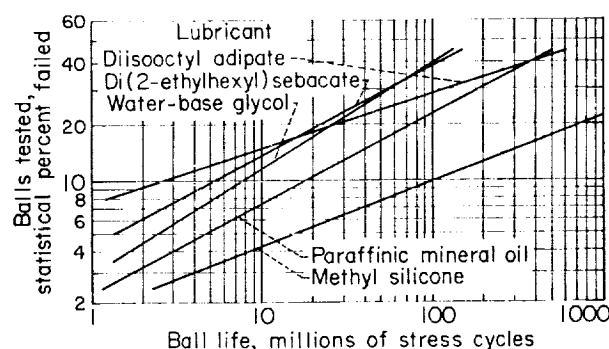


FIGURE 18.—Summary of fatigue lives of ½-inch AISI M–1 tool-steel balls lubricated with various base-stock fluids. Test temperature, 100° F; maximum Hertz compressive stress, 725,000 psi.

cants are distinctly different chemical compounds, they could produce widely different decomposition products and chemical attack at the contacting surfaces. However, no significant evidence of chemical attack on the ball track surfaces was observed in this series of test runs. The running tracks were darkened because of the formation of an oxide film in all but the shortest lived balls. The only variation among these five fluids was a less pronounced track darkening for the glycol run. This darkening of the running track is normal for specimens run in the spin rig, and no significant contrasts were noted among the five lubricant-material groups observed in this test series. No evidence of corrosion pitting or stress corrosion cracking was observed in any of the test specimens during the post-run inspection.

All failures showed the shallow spalling of sub-surface origin characteristic of spin-rig and full-scale bearing failures. No difference was observed among failures produced with the various lubricants.

Metallurgical transformations in the subsurface zones of maximum shear in the contacting bodies are characteristic of materials subjected to a large number of rolling-contact stress cycles. This condition is discussed in detailed later. The alteration of the subsurface material due to deterioration of the metallographic structure could affect fatigue life. However, only slight amounts of transformation were observed at 100° F, and no contrasts were observed among balls run with the different lubricants. Metallurgical transformation was not felt to be a significant factor in the variation in rolling-contact fatigue life observed with the five different lubricants studied.

Since differences in chemical activity, metallurgical transformation, and atmospheric-pressure lubricant viscosity do not appear to be significant factors in causing the wide variation in rolling-contact fatigue life, the effect may be caused by differences in the physical properties of the five lubricants.

As previously discussed, the lubricant film at the rolling-contact zone carries the contact pressure and extends the effective contact area because of viscous shear forces operating at high rolling speeds. This effect reduces the maximum stresses in the contacting elements and hence increases fatigue life. This action is dependent on the viscosity of the fluid in the contact zone, which is under very high pressure. It is known that viscosity increases with pressure and that the rate of increase differs for various base-stock fluids (ref. 17). This viscosity-pressure relation can be approximated by the form:

$$\eta_P = \eta_0 10^{\alpha P}$$

where

$\eta_P$    viscosity at pressure, centipoises

$\eta_0$    viscosity at 1 atmosphere, centipoises

$\alpha$    constant, psi$^{-1}$ (pressure-viscosity coefficient)

$P$    pressure, lb/sq in.

The constant $\alpha$ depends on the fluid base stock and $\eta_0$, and $\eta_P$ is influenced by both $\eta_0$ and $\alpha$. Since $\eta_0$ is constant for the five fluids in this investigation, the controlled variable is fluid base stock. Thus, fatigue life would be influenced by the pressure-viscosity characteristics of the lubricant. If this theory is correct, a correlation should exist between rolling-contact fatigue life and the pressure-viscosity coefficient $\alpha$.

Pressure-viscosity data were not available for

the actual samples of lubricants used in this investigation. Elaborate procedures and equipment are needed for measurement of viscosity at high pressure. Pressure-viscosity data for fluids of the same base stock as those used in this report were evaluated in reference 17. From this source the data for the particular fluids that most closely resembled the fluids used to obtain fatigue data were selected (fig. 19). Average pressure-viscosity coefficients calculated from these relations are given in table II.

A plot of 10-percent life against pressure-viscosity coefficient $\alpha$ is presented in figure 20(a); the same plot for 50-percent life is given in figure 20(b). No point is included for the adipate lubricant because no pressure-viscosity data were available for this fluid. The correlation between the pressure-viscosity coefficient and the 10-percent life is good, and that for the 50-percent
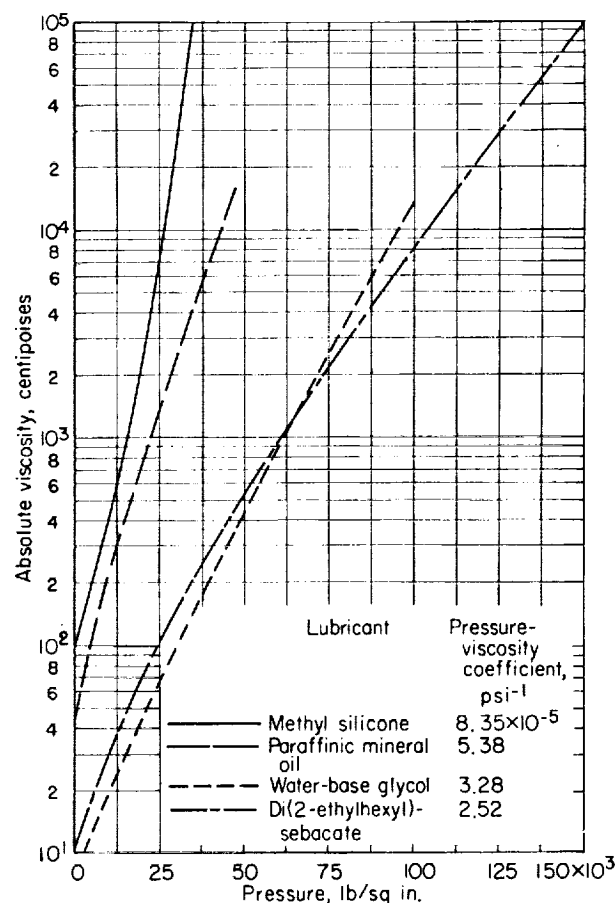


FIGURE 19.—Viscosity as function of pressure for various lubricants (ref. 17). Test temperature, 100° F.
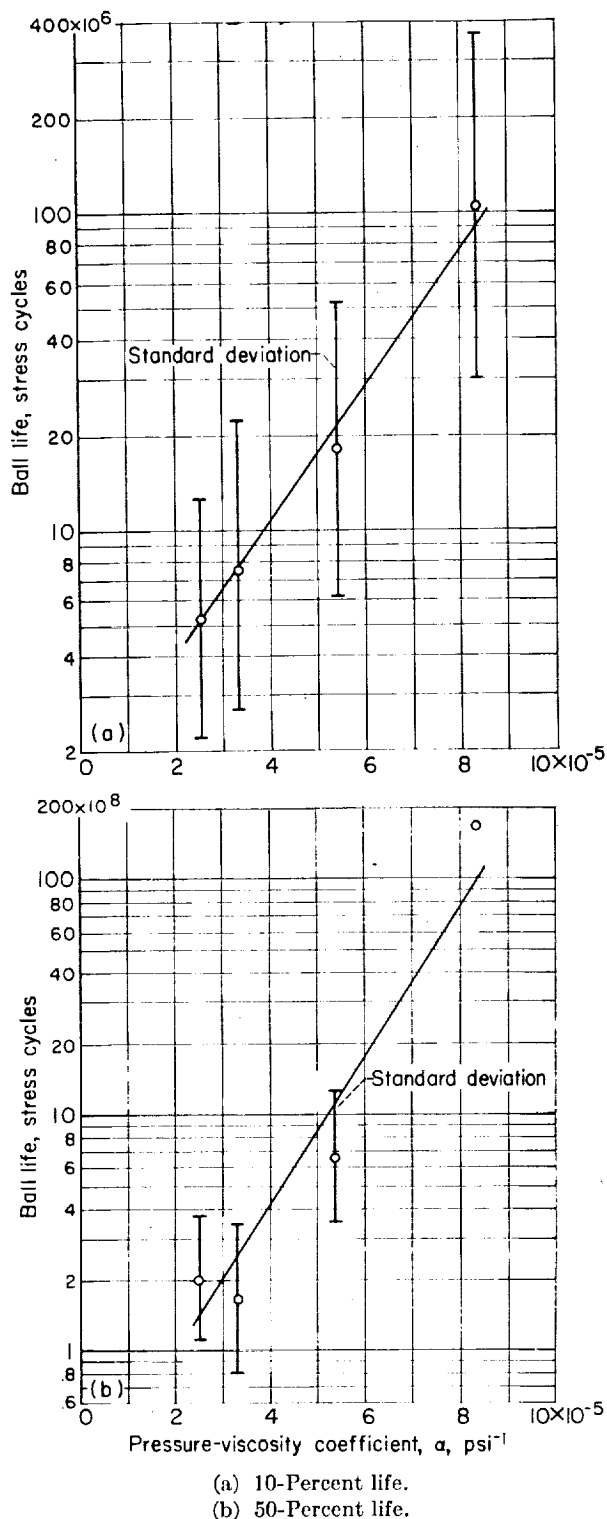
(a) 10-Percent life.
(b) 50-Percent life.

FIGURE 20.—AISI M-1 tool-steel ball life as function of pressure-viscosity coefficient. Test temperature, 100° F; maximum Hertz compressive stress, 725,000 psi; $\eta_P = \eta_o \times 10^{\alpha P}$.

life is fair. This is in contrast to reference 20, in which the authors attempted the same correlation with inconclusive results.

Other lubricant properties also may influence fatigue life. Perhaps bulk modulus or relative chemical activity might be of importance. Although no evidence of chemical activity was found, the least active lubricants (silicone and mineral oil) gave the best life while the most active (adipate and sebacate) gave the poorest life.

Still another factor might be the dynamic response of the viscosity to a sudden change in pressure. At 30,000 rpm in the spin rig, a stress cycle on an elementary volume occurs in approximately $8 \times 10^{-6}$ second. Reference 21 shows experimentally that, 0.001 second after the application of a high pressure, the viscosity of a lubricant is still appreciably below its equilibrum value at the same pressure. Therefore, it seems logical to conclude that the time rate of change of viscosity after the application of a high pressure might be an important property. This time response of viscosity to a pressure change might be significantly different for different base stocks and may not correlate with the ultimate equilibrium pressure-viscosity values. More extensive data and further rheological studies are needed before definite conclusions can be drawn.

The effect of lubricant physical properties on the contact pressures between rolling elements under dynamic conditions, and hence the effect on rolling-contact fatigue life, is directly dependent on the relative rolling speeds of the rolling elements. The rolling speed produced in the spin rig corresponds to a bearing DN value of $1.5 \times 10^{6}$. This is to say that the data on which the preceding conclusions were based were obtained at rolling speeds in the operational range of large aircraft turbine bearings.

The confidence limits for the data were calculated by the method of reference 18 and are presented in figure 20. While wide, they are of a lower order of magnitude than the range of results with the five lubricants. Furthermore, the probability that the four life plots of figure 20(a) would fall in order of ascending pressure-viscosity coefficients is only 1 in 24 if no effect due to lubricant base stock exists. This occurs because calculation by the least-squares, best-fit technique makes these lines objective. Accordingly, the figure-20 results have at least a 96-percent probability not to have been caused by chance.

### EFFECT OF TEMPERATURE

Operating temperature, to the extent that it influences the many factors influencing rolling-contact fatigue life, plays an important role in bearing performance. Both viscosity and pressure-viscosity slope of lubricating fluids decrease with rising temperature (ref. 17). It has been shown in preceding sections that these physical properties have a significant influence on fatigue
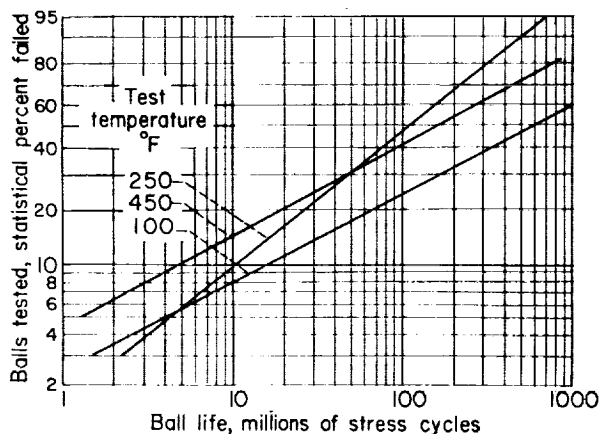


FIGURE 21.—Fatigue life for ½-inch AISI M–1 balls at various test temperatures. Lubricant, di(2-ethylhexyl) sebacate; maximum Hertz compressive stress, 650,000 psi.

life. Other factors such as lubricant chemical activity and stress-induced solid-state reactions in the bearing materials can be influenced by temperature. In order to study the net effect of temperature on rolling-contact fatigue life and to establish a preliminary relation between room-temperature data and higher temperatures of operational interest, a series of tests with temperature as the controlled variable was made.

Tests were run at temperatures of 100°, 250°, and 450° F. Groups of ½-inch-diameter AISI M–1 tool-steel balls (table I) were run on AISI M–1 race cylinders with a synthetic lubricant (di (2-ethylhexyl)sebacate) (table II). Ball loading was held at a level that produced a maximum theoretical Hertz compressive stress of 650,000

psi and a maximum shear stress of 195,000 psi 0.008 inch below the surface.

**Results.**—Life results at the three test temperatures are summarized in figure 21. These results show a reduction in early failure lives with increasing test temperature. On the basis of the relation between life and lubricant viscosity shown in figure 16, some reduction in life can be anticipated because of the change in viscosity of the lubricant film. The table given below shows the theoretical reduction in ball life due to viscosity reduction alone, based on the relation of figure 16.

**Discussion.**—The observed lives were less than those expected if viscosity of the lubricant were the only variable affecting fatigue life. The difference between the observed and the theoretical lives is probably caused by the amplification at the higher test temperatures of other factors affecting fatigue life.

An examination of the fatigue failures produced at 250° and 450° F did not reveal any contrast in appearance or origin with those produced at 100° F. An examination of the running track surface did not reveal any significant evidence of chemical corrosion. At all three temperatures, the tracks exhibited a tendency to darken with increased running time; this is characteristic of spin-rig specimens. Only a slight tendency of this darkening to increase with higher test temperature was observed. All failures were typical spalls limited in area and depth, such as those shown in figure 6.

A deterioration of metallurgical structure in the subsurface zone of maximum shear for SAE 52100 steel previously was reported (ref. 15). This transformation results from the accumulation of hysteresis energy in the shear zone. Metallographic sections of balls run at 100° F showed limited but definite evidence of transformation. Sections of AISI M–1 balls run at 250° F (transverse) and 450° F (longitudinal) are shown in figure 22. On the basis of these sections, it is apparent that the metallurgical structure in the

| Test temperature, °F | Lubricant viscosity, centistokes | 10-Percent life (observed) | 10-Percent life (theoretical) | Life ratio, observed/theoretical | 50-Percent life (observed) | 50-Percent life (theoretical) | Life ratio, observed/theoretical |
|---|---|---|---|---|---|---|---|
| 100 | 13. 5 | 15. 7×10⁶ | ᵃ 15. 7×10⁶ | 1 | 580×10⁶ | ᵃ 580×10⁶ | 1 |
| 250 | 3. 8 | 10. 2 | ᵇ 12. 2 | . 84 | 109 | ᵇ 450 | . 24 |
| 450 | 1. 66 | 4. 75 | ᵇ 10. 3 | . 46 | 160 | ᵇ 382 | . 42 |

ᵃ Assumed the same as observed life.
ᵇ Based on relation $L_1/L_2 = (\eta_1/\eta_2)^{0.2}$, where $L$ is life in stress cycles and $\eta$ is lubricant viscosity.
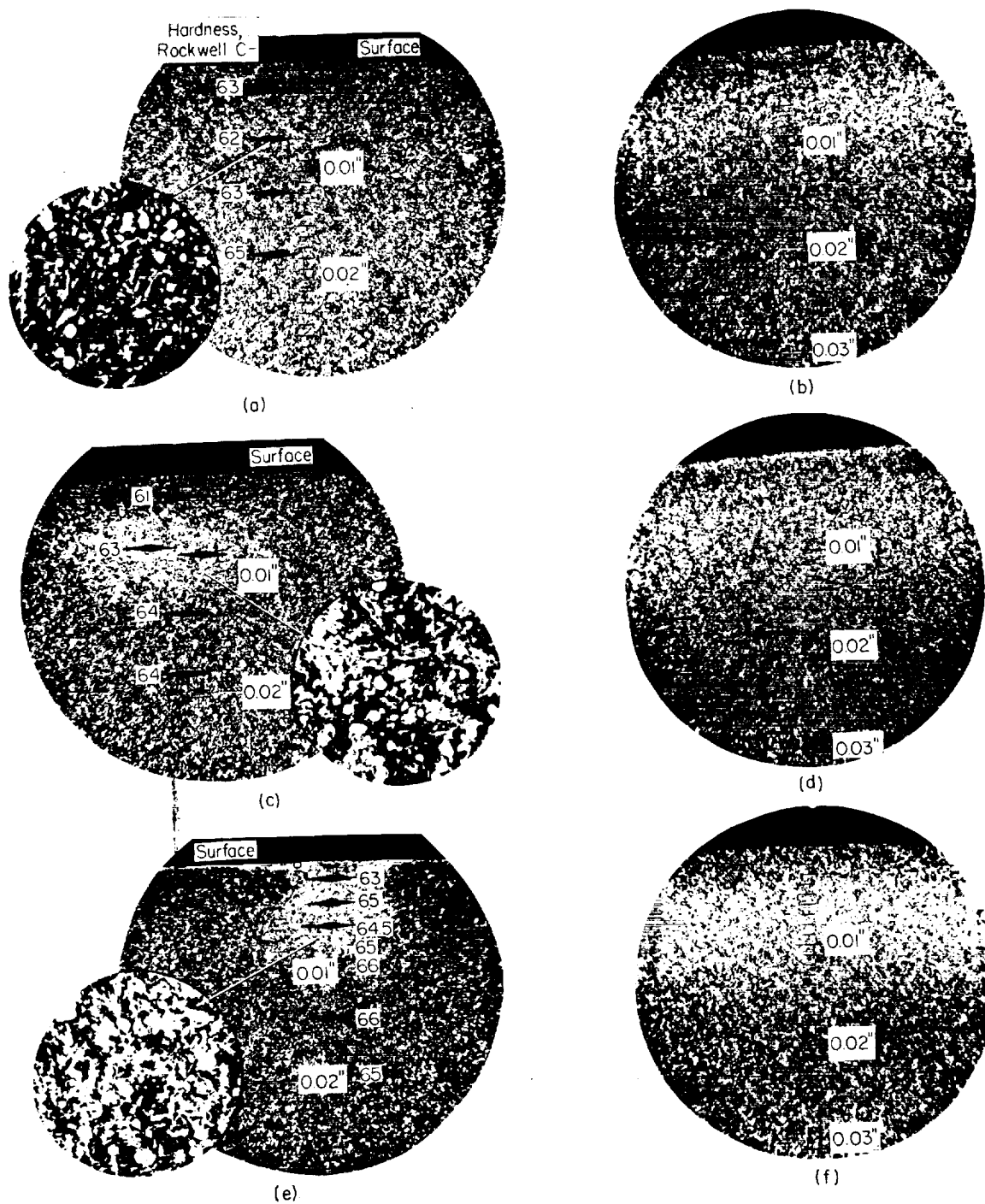
(a)  250° Transverse, 40×10⁶ cycles.

(b)  450° Longitudinal, 21×10⁶ stress cycles.

(c)  250° Transverse, 200×10⁶ cycles.

(d)  450° Longitudinal, 174×10⁶ stress cycles.

(e)  250° Transverse, 1110×10⁶ cycles.

(f)  450° Longitudinal, 261×10⁶ stress cycles.

FIGURE 22.—Metallurgical transformation in subsurface shear zone for ½-inch AISI M-1 balls. Lubricant, di(2-ethylhexyl) sebacate; maximum Hertz compressive stress, 650,000 psi.

subsurface shear zone exhibits a transformation from the original material. This transformation increases with increased number of test cycles and is accelerated by higher ambient temperature. The deterioration of structure in the subsurface shear zone may be one of the factors contributing to the loss in fatigue life at higher test temperatures.

An exception to this temperature reduction in fatigue life is found in the longest lived specimens run at 450° F. It is felt that this disparity is due to the polymerization of the lubricant into a very viscous residue at high temperature. The rate of formation was low, but there was an appreciable accumulation of this substance on the running track after prolonged runs at 450° F. Since viscosity affects fatigue life, the formation of a very viscous film with longer test time would tend to extend fatigue life; and this effect would be more pronounced for longer lived fatigue failures. Lubricant breakdown limited the test temperature feasible with the sebacate base fluid.

### DRY-POWDER LUBRICANTS

Dry powders were used in an attempt to find lubricants usable at test temperatures beyond 450° F. In preliminary test runs when powders were introduced as a dust in air, problems in metering during prolonged, unattended periods were encountered, so that in subsequent tests a suspension of the powder in a fluid that would evaporate at the test temperature was used. A polyalkylene glycol that evaporates at about 350° F and leaves no residue was chosen for the tests run at 450° F. The same heat of AISI M–1 tool steel was used for test specimens as was used in the previous series with the sebacate. The properties of the polyalkylene glycol used in this test series are given in table II. The dry powders used had a maximum particle size of 25 microns. Runs at 100° F were made with a plain glycol and a 0.2-percent suspension of molybdenum disulfide powder in glycol to establish a basis for comparison with high-temperature results. The molybdenum disulfide suspension was then run at 450° F, where the glycol evaporated and left only the dry powder. In these test runs, ball loading was held at a stress level that produced a maximum theoretical Hertz stress of 725,000 psi and a maximum shear stress of 225,000 psi 0.009 inch below the surface. A run with dry

graphite at 450° F was made at a stress level of 650,000 psi in compression and 195,000 psi in shear 0.008 inch below the surface.

**Polyalkylene glycol at 100° F.**—The results for the plain polyalkylene glycol at 100° F are shown in figure 23(a); this run was made to establish a base line for comparison with results for a solid-particle suspension in the fluid. Subsurface metallographic appearance was very similar to that observed previously (in this investigation) with other lubricants for AISI M–1 and to that for other materials at 100° F (ref. 15). However, the track surface did not have the characteristic darkening (due to an adherent oxide film) that was characteristic of all previous material-lubricant combinations tested in the spin rig. This could have been because of abrasion or inhibited oxide formations. Since the track did not show signs of appreciable wear, the latter cause appears more logical. Failure appearance and type were the
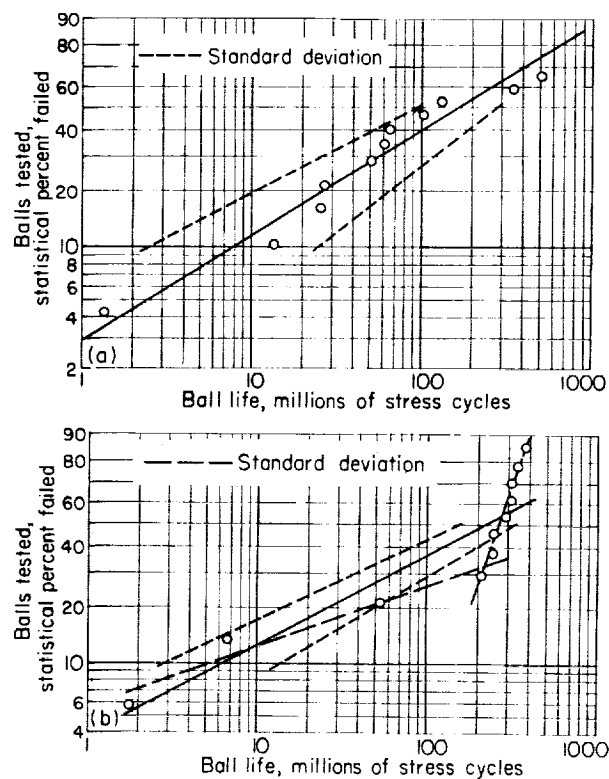


(a) Lubricant, polyalkylene glycol.
(b) Lubricant, 0.2-percent molybdenum disulfide suspension in polyalkylene glycol.

FIGURE 23.—Fatigue life for ½-inch AISI M–1 balls. Test temperature, 100° F; maximum Hertz compressive stress, 725,000 psi.

same as other spin-rig failures and were those common to full-scale bearings. The life results were similar to those produced with the sebacate at 100° F, adjusted for the difference in contact stress.

**0.2-Percent molybdenum disulfide suspension in polyalkylene glycol at 100° F.**—The results shown in figure 23(b) were produced at 100° F for comparison with the pure fluid and with high-temperature results. A best-fit straight line has been drawn through the data points, but obviously this is not a continuous function; and two straight lines (dashed lines) are required to fit the data points reasonably well. The shorter lived specimens apparently produce a curve that is of about the same life and slope as the glycol and other fluid lubricants. However, at about $200 \times 10^6$ stress cycles there appears to be an increase in slope of the fatigue-life curve. This condition produced by a unique type of lubricant (i.e., solid-particle suspension) indicated that the cause of failure may be different at the higher life levels from previously observed fatigue failures with fluid lubricants.

An extensive metallographic investigation was conducted in an attempt to explain the changes in slope of the fatigue-life curve observed at $200 \times 10^6$ stress cycles. Figure 24 shows running-track appearance and longitudinal cross sections of the subtrack region for three specimens subjected to successively greater numbers of stress cycles. Figures 24(e) and (f) show a failed specimen with the complete fatigue spall. This spall is limited in depth and appears to originate in subsurface shear as do normal fatigue spalls observed in the spin rig and in full-scale bearings (fig. 6). However, the depth of origin of the spalls is confined to a zone less than 0.002 inch below the ball surface. A zone of 0.004 to 0.009 inch is considered normal for the failures observed in previous specimens run with simple fluid lubricants. A large amount of cracking was observed at a depth of much less than 0.001 inch (fig. 24(g)). Incipient cracking and matrix damage originating from carbides were more common and more agglomerated than in previous specimens. This indicated both higher local stresses and non-uniform stressing. Structural changes characteristic of the subsurface zone of maximum shear tended to be less severe and closer to the surface. A strong tendency for formation of surface

cracking was observed in these three specimens (figs. 24(b), (d), and (f)). This condition is not typical of fluid-lubricant fatigue failures. The cracking had a characteristic pattern that bore a definite relation to the relative sliding always encountered in rolling contact of a ball with a race. Since the radius of rotation is at a maximum at the running-track center and is progressively less toward the outside, while the angular rotation is the same, the surface speed must vary in the transverse direction; this causes relative sliding of the surfaces. To maintain an overall rolling of the ball, the sum of the friction forces generated at the contact zone must equal the tangential force in the direction of rolling; otherwise, the ball would accelerate. Thus, the sliding is opposite the rolling direction at the center of the ball and in the same direction at the track edges. At some point in between, the relative sliding of the two surfaces is zero. Thus, there are two bands of pure rolling on the track. The cracking in figures 24(b), (d), and (f) has an abrupt change in direction at these bands of pure rolling. Thus, it has a characteristic pattern relative to surface sliding.

The shallow depth of subsurface crack origin (figs. 24(a), (c), and (e)) and the surface crack pattern (figs. 24(b), (d), and (f)) indicate a much stronger skin effect in the suspension-lubricated balls than that observed in fluid-lubricated balls. High shear stresses are apparently generated at the surface by the relative sliding of the contact surfaces; this is in addition to the high shear stress that results from the compressive stresses, which is a maximum about 0.009 inch below the surface. Since the rate of relative sliding and contact pressures is the same for this test run as for previous fluid-lubricated runs, the effective friction coefficient apparently is higher for the solid-particle-suspension lubricant.

Evidence of corrosion at the contact surface was very strong in this test run. All previous fluid-lubricated runs yielded very limited evidence of contact surface corrosion. Figures 24(b), (d), and (f) show this pitting and the tendency for it to aline with the surface cracking. Apparently there is an interaction between surface corrosion and the cracking, with each one promoting the other. Cracking, or the high local stresses causing cracking, would facilitate corrosion; and a corrosion pit would provide the stress concentra-
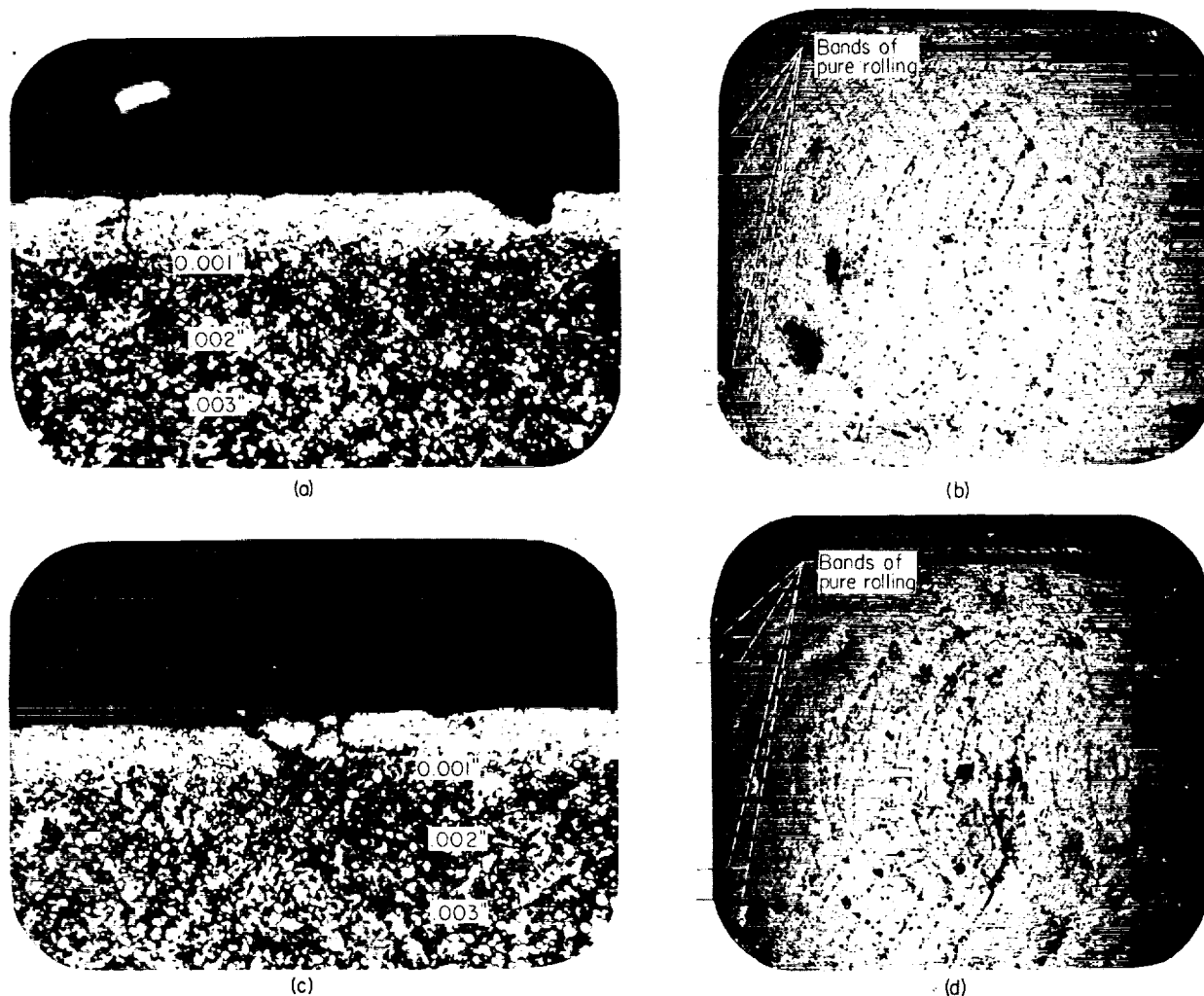
(a) Longitudinal section; X500; 53×10⁶ stress cycles.
(b) Ball surface; X75; 53×10⁶ stress cycles.
(c) Longitudinal section; X500; 210×10⁶ stress cycles.
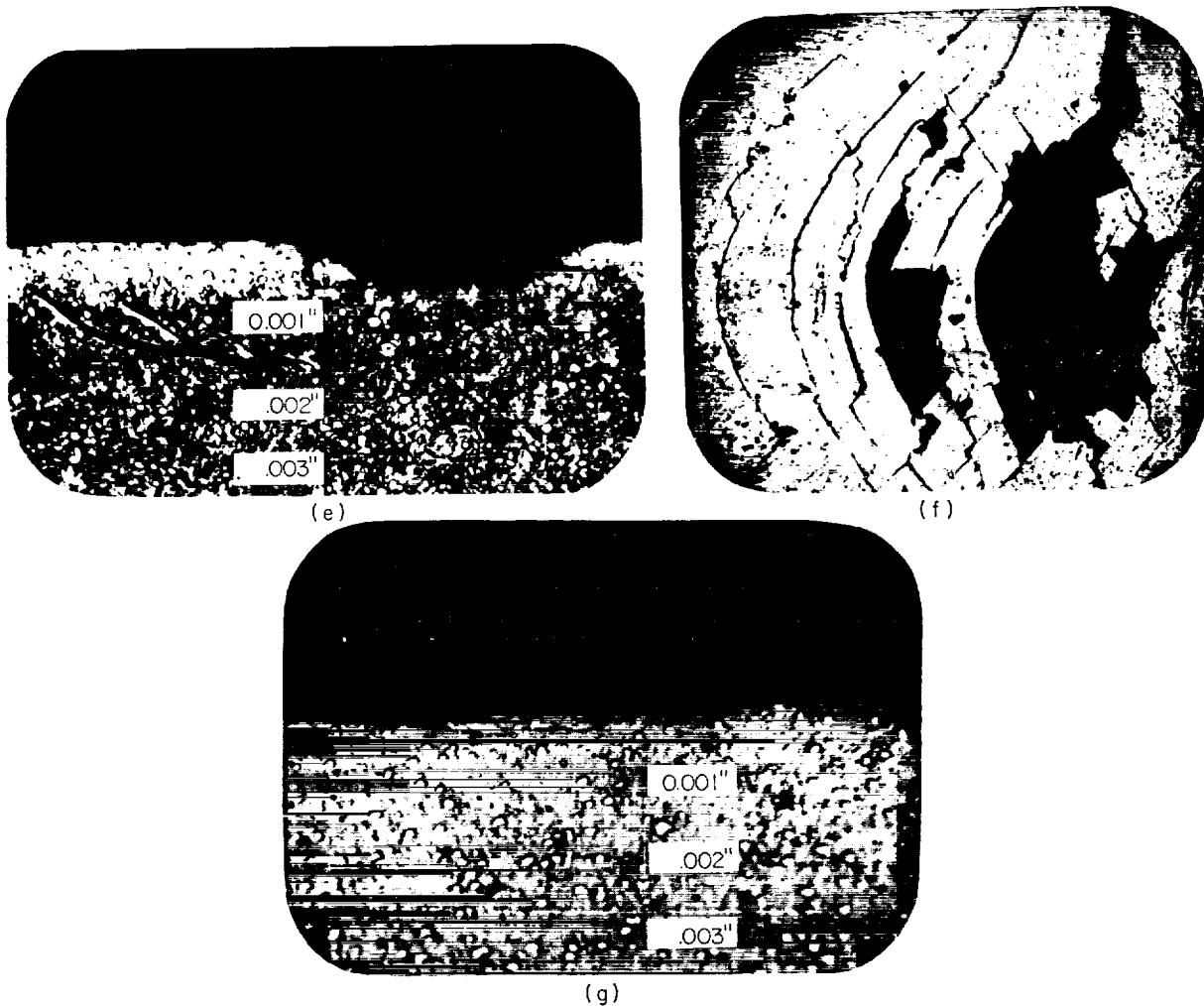(d) Ball surface; X75; 210×10⁶ stress cycles.

FIGURE 24.—Typical specimens. Lubricant, 0.2-percent molybdenum disulfide suspension in polyalkylene glycol; M-1 tool steel; test temperature, 100° F; maximum Hertz compressive stress, 725,000 psi.

tion for fatigue cracking. Figures 24(a) and (c) present a cross section of the ball subsurface showing the penetration of corrosion cracking into the subsurface. The increase in depth with longer test time is apparent. These corrosion cracks generate secondary cracking parallel to the surface, which is the normal cause of fatigue spalling. A typical spall is shown in figure 24(c).

The formation of very small fatigue spalls is shown in figure 24(d). These fine spalls are too small to cause enough vibration for failure shutdown, but they are of interest because of their unique tendency to form at the bands of pure rolling. This observation, together with the indication that higher than normal localized stresses were present, as indicated by agglomerated incipient failures (fig. 24(d)), indicated that some stress-raising effect was acting in the bands of pure rolling. This could be the solid lubricant particles in the suspension. This observation is developed further in the discussion of the next test series.

The abrupt change in slope of the fatigue curve observed in figure 23(b) for the molybdenum

(e) Longitudinal section; X500; 330×10⁶ stress cycles.

(f) Track surface; 330×10⁶ stress cycles.

(g) Longitudinal section; X500; 53×10⁶ stress cycles (unetched).

FIGURE 24.—Concluded. Typical specimens. Lubricant, 0.2-percent molybdenum disulfide suspension in polyalkylene glycol; M-1 tool steel; test temperature, 100° F; maximum Hertz compressive stress, 725,000 psi.

disulfide—polyalkylene glycol suspension appears to be caused by an interaction of stress corrosion and the high surface shear stresses due to skin effect. The higher shear stress generated by surface sliding would tend to move the maximum shear stress nearer the surface than would be normal for that resulting from compressive stresses alone. The corrosion cracking progresses from the surface at a relatively constant rate. When it reaches the critical zone (i.e., high shear stress) where fatigue spall cracking originates, the susceptibility for fatigue failure is greatly increased, and a large

fatigue spall will soon develop. If the time for corrosion cracking to proceed to this depth corresponds to the running time for 200×10⁶ to 400×10⁶ stress cycles (region of increased slope in fig. 23(b)), the concentration of the longer lived failures within this range could be expected.

**Dry molybdenum disulfide powder at 450° F.—** The results shown in figure 25(a) were produced at a test temperature of 450° F with molybdenum disulfide suspended in polyalkylene glycol. The glycol evaporated at approximately 350° F and left a dry powder at the test temperature.
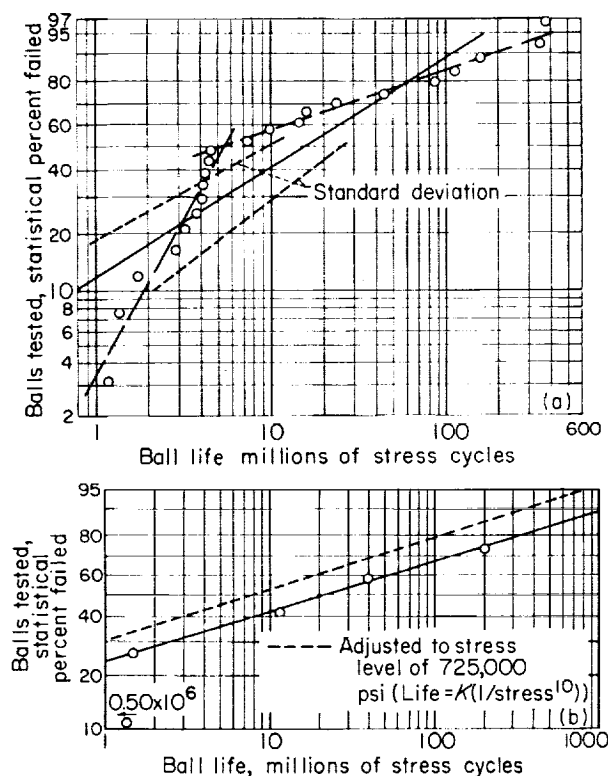
(a) Lubricant, 0.2-percent molybdenum disulfide suspension in polyalkylene glycol: maximum Hertz compressive stress, 725,000 psi.

(b) Lubricant, graphite-air dust; maximum Hertz compressive stress, 650,000 psi.

FIGURE 25.—Fatigue life for ½-inch AISI M-1 balls. Test temperature, 450° F.

A best-fit straight line was drawn through the data points of figure 25(a), but again, as for the molybdenum-disulfide-suspension results at 100° F, it is obvious that two straight lines (shown as dashed lines) are required to fit the data points reasonably well. In these tests, the time required to reach the test temperature was about 30 minutes. Since heat is supplied by the drive air, preheating was not practical. A running time of 30 minutes corresponds approximately to the intersection of the two dashed lines, so that the lower dashed line corresponds to a transition from room temperature to 450° F. Once the test temperature was reached, the slope changed and produced the results considered to be a measure of AISI M-1 tool steel lubricated with dry molybdenum disulfide powder at 450° F.

The life observed at these test conditions was

poorer than that observed at the same test temperature with the sebacate fluid (fig. 21) after adjusting the life to correct for stress differences. The disparity in life is even greater when comparing with room-temperature results. Apparently some new and adverse factor, which did not exist with a fluid lubricant, is influencing fatigue life.

**Dry graphite powder at 450° F.**—In order to evaluate possible chemical corrosion action as a failure-causing factor, a comparison can be made with test results produced with dry graphite powder. Since graphite is quite different from molybdenum disulfide chemically but similar physically, different results would be expected if chemical activity were a major factor in ball fatigue life. The results shown in figure 25(b) were produced at 450° F with dry graphite powder. These tests were run at a lower stress level (650,000 psi) than the molybdenum disulfide runs previously discussed; however, an adjustment can be made to the stress level of the molybdenum disulfide run (725,000 psi) by the relation, life$=K$ $(1/\text{stress})^{10}$, established for the spin rig in figure 4. The number of data points is limited because of the problems encountered in metering the graphite-air dust, but the close proximity of the points to a straight line indicates that the results may closely
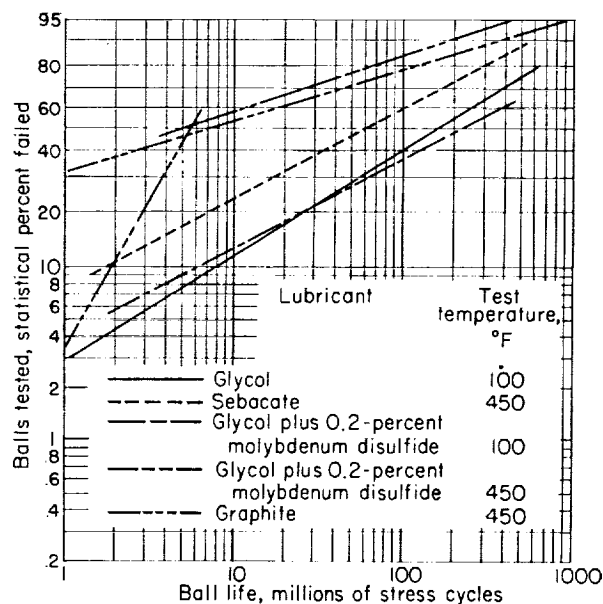


FIGURE 26.—Fatigue life for ½-inch AISI M-1 balls with various lubricants. Maximum Hertz compressive stress, 725,000 psi.

approximate the results for a greater number of points. Since no fluid was present at the test temperature and the particle size was about the same for both powders, the molybdenum disulfide and graphite powder lubricants closely resembled each other physically.

**Comparison of results with fluid and dry-powder lubricants.**—Figure 26 is a comparison of the Weibull plots for the two dry powders with each other and with fluid lubricants, all at the same stress level. Fatigue life was lower at 450° F than at 100° F. The similarity of results for the two dry-powder lubricants that have greatly different chemical characteristics appears to minimize the importance of chemical corrosion as a factor causing rolling-contact fatigue failure under these test conditions. One possible reason for this apparent anomaly is the lack of a fluid film to hold corrosive substances at the contact surfaces. Volatile sulfur oxides would be removed by the air blast if not held in solution. Figure 27(a) shows no evidence of corrosion pitting as compared with that noted at 100° F (figs. 24(b) and (d)). While the two test runs with dry-powder lubricants at 450° F produced similar results, they are much different from the results for the fluid sebacate at

450° F and for the fluids and suspensions at 100° F.

The metallographic transformation in the subsurface zone of maximum shear for both molybdenum disulfide and graphite lubricated balls is similar to that characteristic of rolling-contact fatigue specimens in general. The light etching area of figure 27(b) is similar to that observed with a sebacate fluid at 450° F (fig. 22). Metallographic changes do not appear to be the cause of the lower life.

The most logical explanation of the low rolling-contact fatigue life produced with the dry powders appears to be in mechanical rather than chemical effects. Both the dry powders produced failures that were mutually identical in appearance, yet entirely different from those observed with the fluid lubricants. Figure 27 illustrates this point: A pattern of two annular bands of spalling was observed on the ball track. These bands were coincident with the bands of pure rolling that are present in all spheres rolling on a cylindrical surface. These spalls in the bands of pure rolling are similar to the normal fatigue spall except that they are on a much smaller scale. They appear to originate from subsurface shear cracking as do normal spalls. A tendency for small spalls to
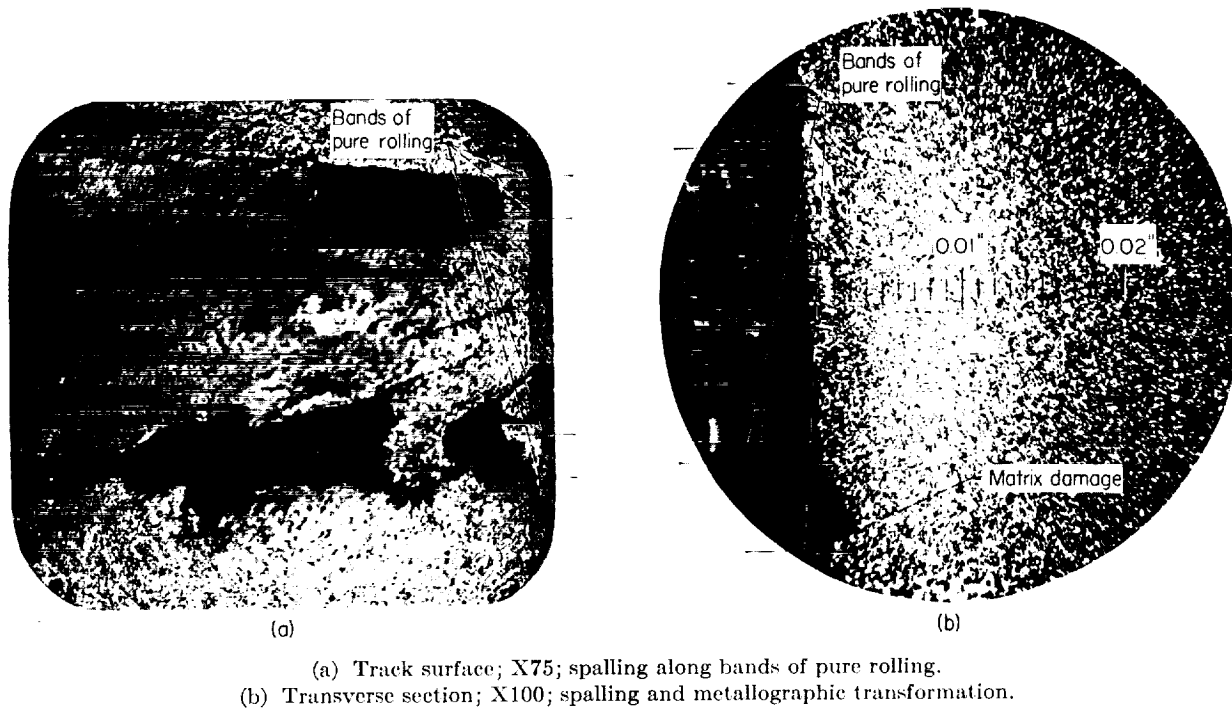


(a) Track surface; X75; spalling along bands of pure rolling.
(b) Transverse section; X100; spalling and metallographic transformation.

FIGURE 27.—Typical dry-powder failures. AISI M–1 tool steel; powder lubricant, molybdenum disulfide; test temperature, 450° F; maximum Hertz compressive stress, 725,000 psi.

form in the bands of pure rolling was noted previously with the molybdenum disulfide suspension at 100° F (fig. 24(d)). A metallographic examination showed that the incipient failures, and matrix damage originating from carbides, tended to be more common and more segregated than in balls tested with fluid lubricants; this result indicates that high localized stresses were present. Localized matrix damage was observed in visual inspection of sections such as figure 27(b). These localized areas tended to be under the bands of pure rolling; this indicates that a stress raiser was acting in the bands of pure rolling. If an even pressure distribution were present, the maximum pressure would be at the center of the track, and the first sign of failure would be expected there.

Apparently the lack of relative sliding of the contacting surfaces at the bands of pure rolling enables the dry-lubricant particles to retain some of their shape, while the sliding in the remainder of the contact area smears the particles into a smooth, continuous lubricating film. This phenomenon is illustrated schematically in figure 28. The pressure distribution with a fluid lubricant (fig. 28(a)) is smooth and reaches a maximum at the center of the contact ellipse. This is the typical pressure distribution for a sphere in contact with a cylinder, as computed from reference 9.

The existence of a dry particle that is larger than the average thickness of the lubricating film formed by the smearing action would produce



(a) Fluid lubricant.
(b) Dry-powder lubricant.

FIGURE 28.—Transverse-section diagram of pressure distribution in rolling sphere. Ball motion out of paper toward reader.

the effect shown in figure 28(b). Since, at bands of pure rolling, the relative motion of the two surfaces is perpendicular to the plane of the surfaces, all stresses on the lubricant particles would be in compression. The particles would tend to be deformed to the average film thickness by compressive forces. The particles could bear compressive stresses higher than their normal yield strength for the same reason that the balls carry stresses far above their normal yield strength through what is essentially hydrostatic loading; that is, the material has no place to which to flow. Particle size, not investigated here, may have an important influence. A mathematical analysis of this phenomenon would be very complex, if not impossible.

The theory that the dry-lubricant particles produce high, localized compressive stresses in the bands of pure rolling is a hypothetical one, but there is a substantial amount of evidence indicating that some type of localized stress raiser that was not present in fluid lubricants is present with dry lubricants. The unique appearance of the spalling, intense localized incipient matrix damage confined to the region of the unique spalling, and the short lives all indicate that this is the case. Since a complete bearing has better conformity between ball and race, hence greater relative sliding of the surfaces, the observed effect of dry-powder-lubricant particles acting as stress raisers may be reduced to a negligible role in normal rolling-contact bearing applications.

### METALLOGRAPHIC STRUCTURE

Fatigue spin-rig specimens provide ideal material for detailed metallographic investigations because all stressing is confined to a single great circle track that is known in advance. This greatly reduces the volume of material requiring sectioning. The results reported herein were obtained from specimens produced by various fatigue-life tests in the spin rig.

Inclusions and incipient failures.—Investigation showed that inclusions contribute to ball fatigue failures and life scatter. Inclusions under the ball tracks to an average depth of 0.028 inch are metallurgical stress raisers that initiate cracks. These cracks enlarge and propagate under repeated stress and become potential
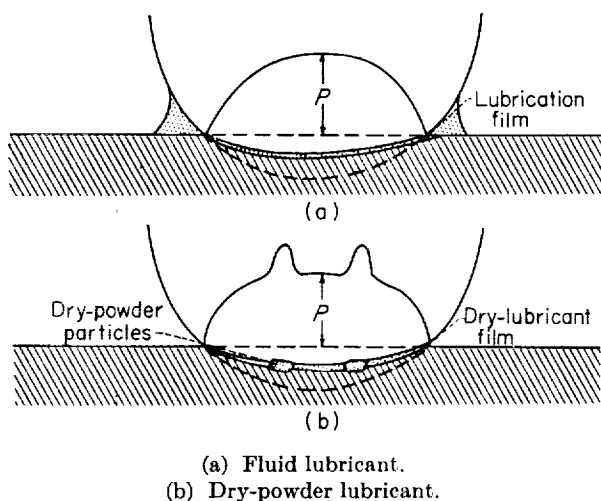
failures varying in degree as shown in figure 29.

Figure 29(a) shows representative inclusion damage about which the following observations can be made:

(1) These cracking conditions are the rule rather than the exception.

(2) The angles of cracking generally are approximately 45° to normal; that is, they are in the maximum-shear plane.

(3) When inclusions are segregated, there is a tendency toward crack alinement.

The ball of figure 29(a) was tested for $410 \times 10^6$ cycles without failure, so these defects are not too serious. However, figure 29(b) shows the damage that a single, medium-sized (0.0015-in. diam.) inclusion can do in approximately $80 \times 10^6$ cycles, even though it is located appreciably deeper than the maximum-shear-stress area.

Balls have a very hard matrix that is sensitive to loading and environmental variables. Imposed thereon during fatigue testing is a complicated and cyclic stress pattern. Therefore, close correlation of incipient cracking with running time could not be expected.

Qualitative generalizations can be made if it is noted that the location of an inclusion with respect to the maximum shear stress is of prime importance. Observations regarding inclusions common to both SAE 52100 and AISI M-1 are as follows:

(1) Inclusion hardness affected the amount of matrix cracking. The softer sulfides produced less matrix cracking than the harder oxides. Occasionally very hard, angular, yellow-colored inclusions, probably a nitrogen-rich solid solution of titanium nitride and titanium carbide, caused the most severe cracking conditions. All of these inclusion types are shown in figure 29(c).

(2) Crack initiation begins within $10 \times 10^6$ cycles. With increased running time, more inclusions became affected; thus, there was a general trend toward an increased amount and degree of cracking. Steel cleanliness is, of course, another variable.

(3) Effects of variation in inclusion size are depicted in figure 29(d). Small laminations found only in AISI M-1 steel can be serious hazards (see fig. 29(e)).

(4) In balls with short test runs ($80 \times 10^6$ cycles), inclusions caused matrix cracking under the

stressed track to a depth of approximately 0.023 inch; this depth increased to 0.040 inch in long tests.

There were also variations in the effect of inclusions between SAE 52100 and AISI M-1 materials. Inclusions were more numerous in SAE 52100 steel; however, the majority were of the less harmful sulfide type. Although oxides initiated severe local matrix cracking in SAE 52100, crack propagation was less than that with AISI M-1 steel. No instances of crack propagation such as shown in figure 29(b) were encountered in SAE 52100 steel.

Figure 29(f) shows comparative matrix cracking produced by an oxide and by a sulfide inclusion in an SAE 52100 ball tested at room temperature. This figure also shows that, although the matrix was severely cracked, crack propagation was limited, since this ball had a longer than average life of $450 \times 10^6$ cycles.

Compared with balls run at room temperature, the incidence of inclusion cracking at 250° F was much decreased in SAE 52100 steel. The sulfides seldom initiated cracking, and only the larger, more critically located oxides caused matrix cracking.

In AISI M-1 steel the carbides are larger and also cause incipient failure similar to inclusions. This is shown in figures 29(g) and (h); (g) is a segregated carbide streak in a ball pole area, and in (h) the large carbide has been split in half by the concentrated high stresses. Note also that, with normal etching, the incipient failure progressing from the split carbide shows no cracking and remains unetched. Likewise, the damaged matrix caused by the heavy scratch to the lower right remains unetched and so indicates a similar severe straining condition in contrast to the brittle matrix cracking observed in SAE 52100 balls (fig. 29(c)).

Some of the incipient failure regions, as in figure 29(i), were large enough for hardness measurements and showed hardnesses approximately three Rockwell C points higher than the surrounding matrix; this again indicates severe straining. In order to further establish the nature of such areas, the specimen was etched with electrolytic chromic acid (fig. 29(j)); this showed that these failure areas are a combination of very fine cracks and amorphous metal.
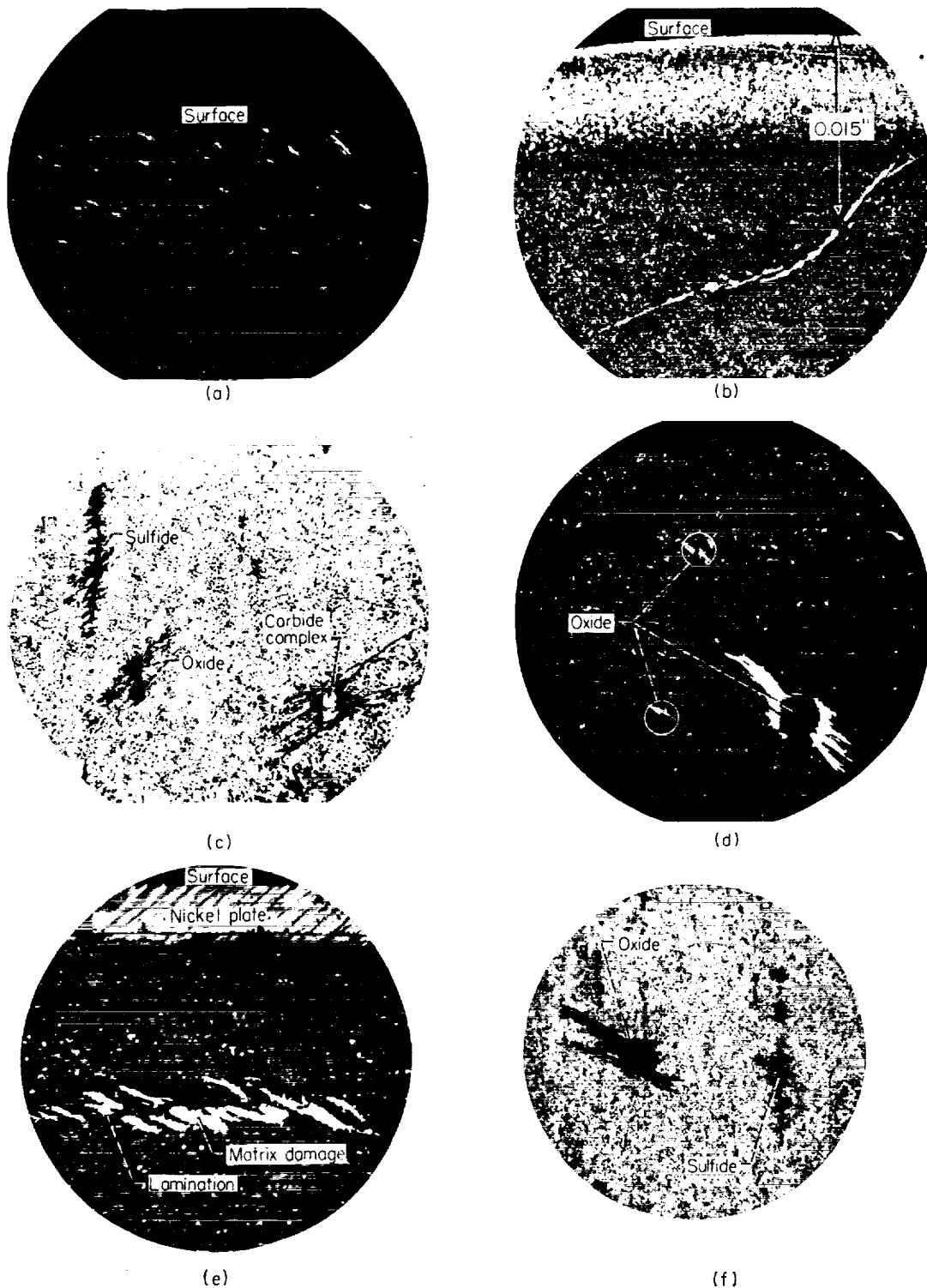
(a)  Small matrix cracks caused by inclusions in AISI M–1.   X75; 410×10⁶ cycles.
(b)  Crack propagation from large inclusion in AISI M–1.   X75; 80×10⁶ cycles.
(c)  Relative matrix cracking incurred by carbide, **oxide**, and sulfide inclusions in SAE 52100.   X500.
(d)  Inclusion size effects and cracking in AISI M–1.   X250.
(e)  Matrix damage (white) caused by lamination (black) in AISI M–1.   X500.
(f)  Brittle type of matrix cracking in SAE 52100.   X250; 450×10⁶ cycles.

FIGURE 29.—Inclusions and incipient failures.
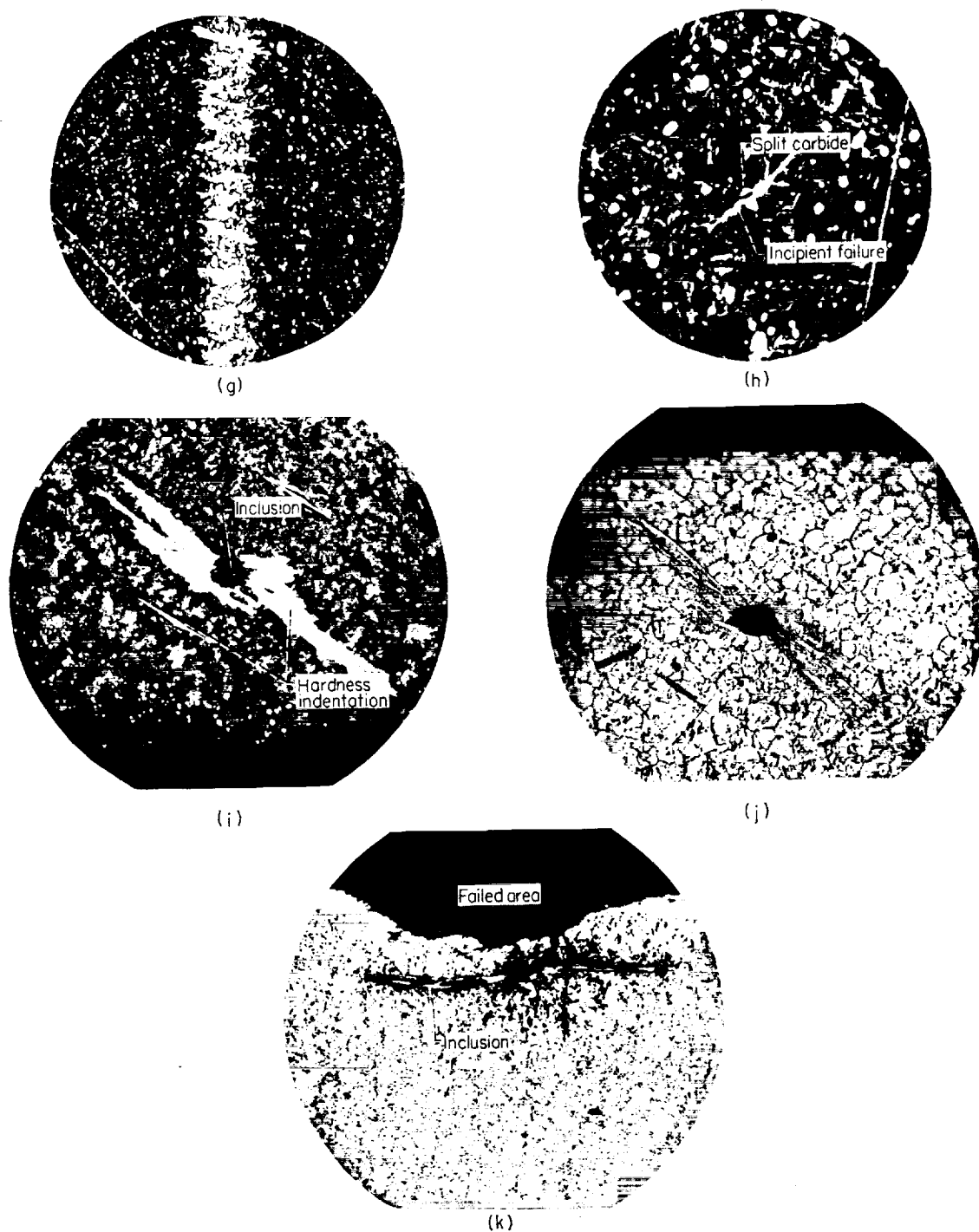
(g) Segregated carbide streak and matrix damage in AISI M-1.   X500.

(h) Incipient failure progressing from a carbide (split) inclusion in AISI M-1.   X1500.

(i) AISI M-1 matrix damage (white) showing no cracking with picral-HCl etch.   X500.

(j) Same as (i) after additional etching with chromic acid (electrolytically); shows small cracks and amorphous structure.

(k) Fatigue failure caused by inclusions in SAE 52100.   X250.

FIGURE 29.—Concluded.   Inclusions and incipient failures.

The oxides in AISI M-1 were more numerous than in SAE 52100 and frequently were segregated, so that small laminations (fig. 29(e)) were caused. The incidence of incipient cracking around all inclusions showed a slight decrease at the 250° F testing temperature. However, crack propagation, which showed a decided decrease at 250° F for SAE 52100 balls, was appreciably increased in AISI M-1 balls.

Inclusions in this study were shown to cause stress concentrations resulting in incipient failures of varying degree. Although the majority of matrix cracking observed did not terminate in a ball fatigue failure, inclusions are responsible for some failures. Figure 29(k) shows a ball failure attributed to the designated inclusion.

Inclusion and material characteristics are summarized as follows:

(1) Inclusion location is of primary importance. Size and orientation are also important.

(2) The oxides and larger carbides are more harmful than the softer sulfide inclusions.

(3) A decided decrease in crack formation was shown for SAE 52100 with increase of testing temperature from room temperature to 250° F.

(4) In AISI M-1 a slight decrease in matrix crack formation was observed at 250° F. How-

ever, a decided increase in crack propagation tendencies was indicated.

(5) The nature of incipient failures in AISI M-1 indicated a more ductile matrix than in SAE 52100 steel.

(6) Inclusions, carbides, and matrix conditions appeared slightly less harmful to fatigue in SAE 52100 balls than in AISI M-1 balls.

**Subsurface structural changes.**—Metallurgical structure changes in the cyclically stressed region immediately below the running track were observed previously in SAE 52100 steel (ref. 15), and a brief résumé of this effect with AISI M-1 is given in the preceding section on temperature (p. 24). A more detailed investigation was made with SAE 52100 steel specimens.

At room temperature, no significant effect of repeated stressing was observed in SAE 52100 balls after long runs at 714,000-psi maximum compressive Hertz stress, aside from the inclusion damage already discussed. Figure 30 gives comparison photomicrographs of an untested ball and another ball after a test run for $2000 \times 10^6$ cycles without failure.

At 250° F, marked changes in the metallurgical structure of the high-shear-stress region were observed in balls run at 633,000-psi maximum



(a)    (b)

(a) As received.
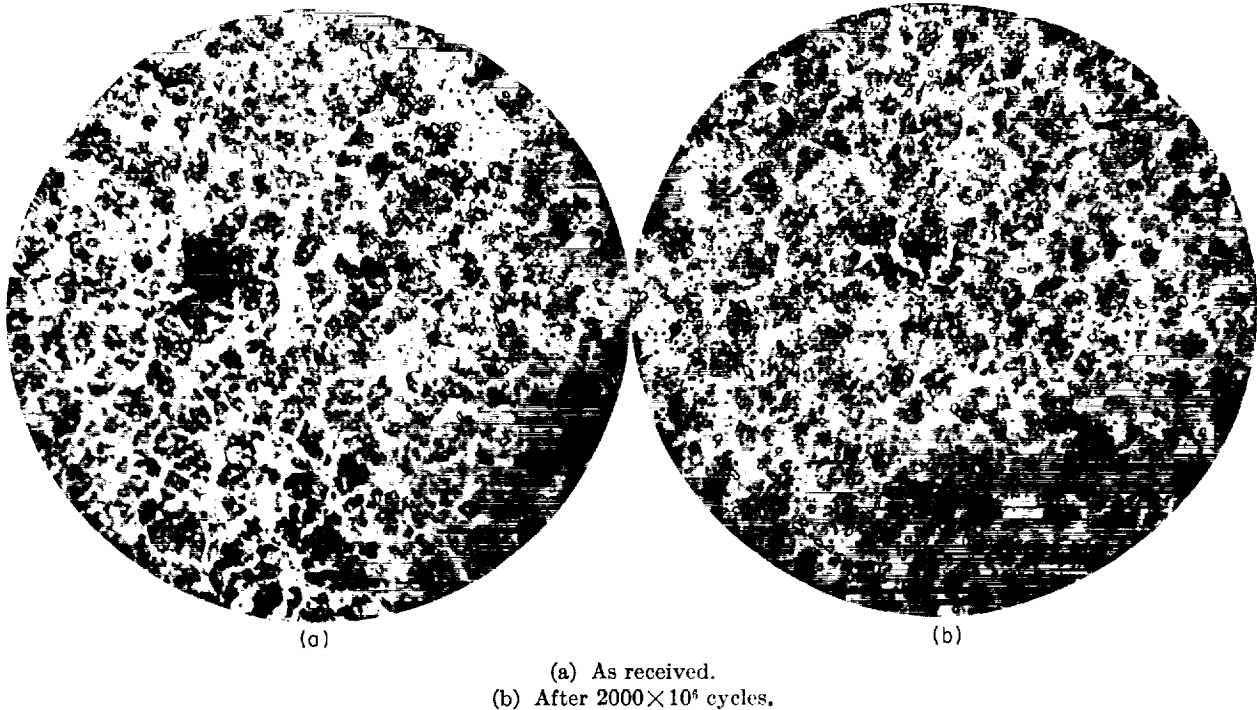(b) After $2000 \times 10^6$ cycles.

FIGURE 30.—SAE 52100 microstructures before and after testing at room temperature. X750.

compressive Hertz stress. Such changes in structure formed a dark etching band in the subtrack zone. This condition is shown in figures 31 to 33, representing $30 \times 10^6$, $100 \times 10^6$, and $310 \times 10^6$ stress cycles; figures 31 and 33 are sections longitudinal to the running track, while figure 32 is a transverse section.

The changes of structure are the results of additional tempering to a stage called troostite. A combination of thermal and strain energy in the maximum-shear-stress regions of the ball is believed to cause the change. Comments on the various features of this condition, as shown in the composite photomicrographs, are itemized as follows to simplify reading and reference.:

(1) The background photographs of figures 31 to 33 are section views of a ball diameter and show the bands to be uniform in density and width. The inset views with the included micrometer scale enable band measurements to be made. Distances shown are depth in inches below surface. They also show limited structure detail and Tukon indentations. Inset views magnified 750 times are included to show the structure detail in the troostite areas.

(2) The edges of these bands are acicular, occasionally with directional tendencies as shown in inset C of figure 31. This is believed to be an intermediate condition of tempering because it is more prominent in balls with short testing times. Inset C of figure 31 also includes an incipient failure with an entrapped area of dark etching matrix, which raises a speculative question: What was the source of the energy that caused a local increase in structure change in this area? This energy is probably caused by stress concentrations at a small local defect.

(3) From the amount of band formed in $30 \times 10^6$ cycles (fig. 31), this structure change apparently begins soon after test initiation. With increased time, the troostitic bands become wider and more dense, as a comparison of figures 31 and 33 indicates.

(4) In the areas between the ball surface and the bands, such as area Y in inset B of figure 32, no structure change could be detected; although a slight softening, compared with average matrix hardness, was usually indicated. These hardness

results are discussed in item (5) of the hardness summary (p. 45). In long runs, such as the $310 \times 10^6$ cycle run of figure 33, this area between the band and the surface also becomes troostitic. This is the area labeled Y in inset D of figure 33, and the structure is identical to that of the band (area W). There is a meeting of bands at area X on this photomicrograph because of band widening and structural change under the ball track.

(5) In about $100 \times 10^6$ cycles, many very fine cracks develop in the troostitic areas. Insets A and D of figure 32 show such cracks; they are partially obscured by the dark matrix etching, however. In this transverse view, the cracks are parallel to the track, being more numerous in the center of the elliptical band. With longer running times, these shear cracks enlarge and elongate as in inset A of figure 33; inset B is a higher magnification of these shear cracks. In this longitudinal view the shear cracks are at an angle of 45° to the ball track and presumably result from the reduced strength caused by the structure change.

(6) The hardness decrease in the troostitic areas was less than expected. A Rockwell C hardness of 61 was measured, compared with an average ball hardness of Rockwell C–63 to –64 for the unchanged structure.

(7) The ball failures included in figures 31 and 32 are typical of those encountered at 250° F. They are shallow, showing a tendency not to penetrate into the troostitic band but rather to skim along the edge. This tendency may be caused by collapse of the harder layer, resulting from insufficient support from the softer underlying troostite.

Although the etching characteristics (color) are reversed, the bands of transformed structure in 52100 are similar to AISI M–1 (fig. 22). In both SAE 52100 and AISI M–1 they become more prominent with increased stress cycles and higher test temperature. Size and area of origin of the bands are similar in both materials.

Skin effects, of which area Y (fig. 33, inset D) is representative, were observed only in the longer running SAE 52100 balls tested at 250° F; but they occurred more frequently in AISI M–1 steel. This structure change was less than 0.001-inch
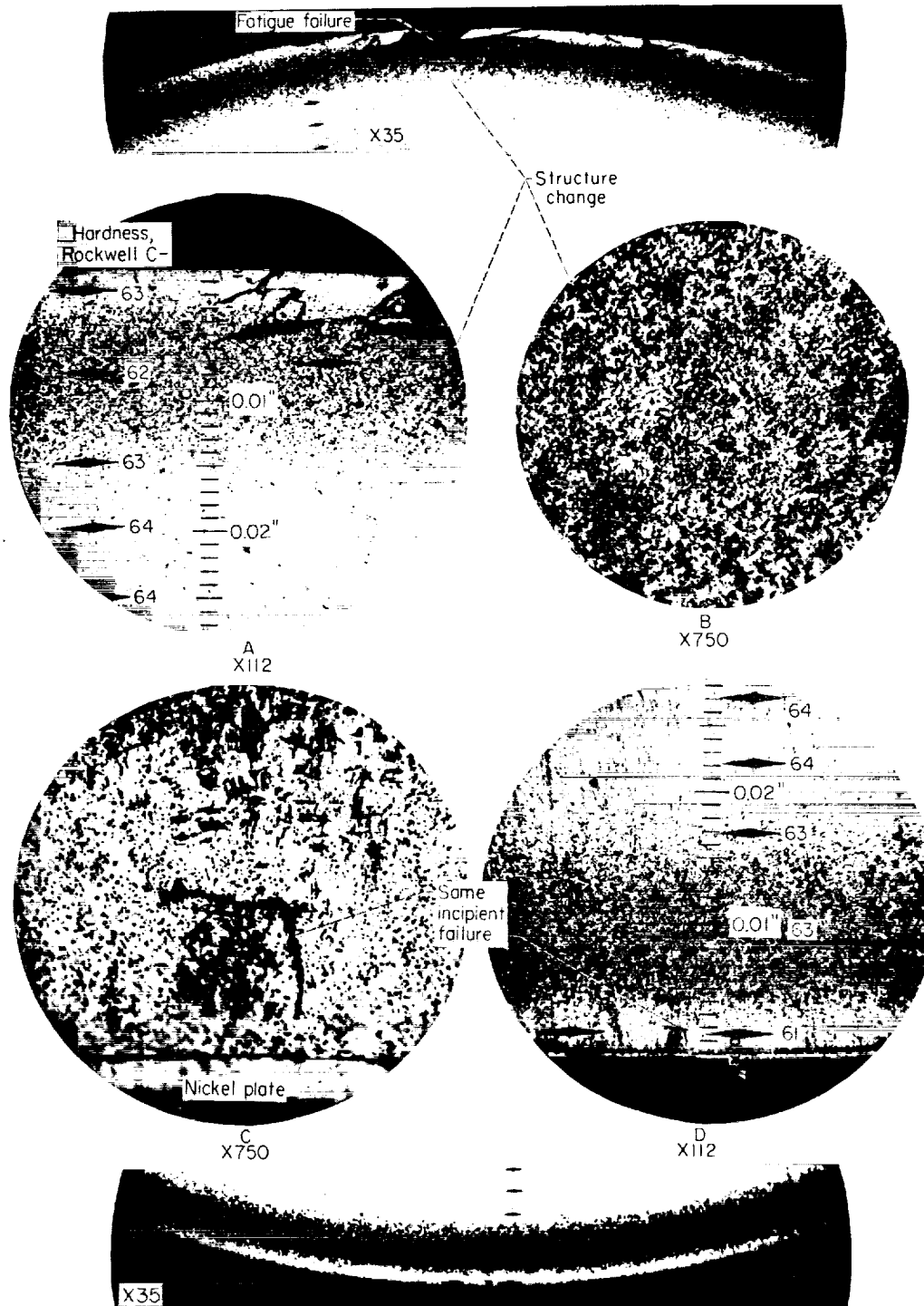
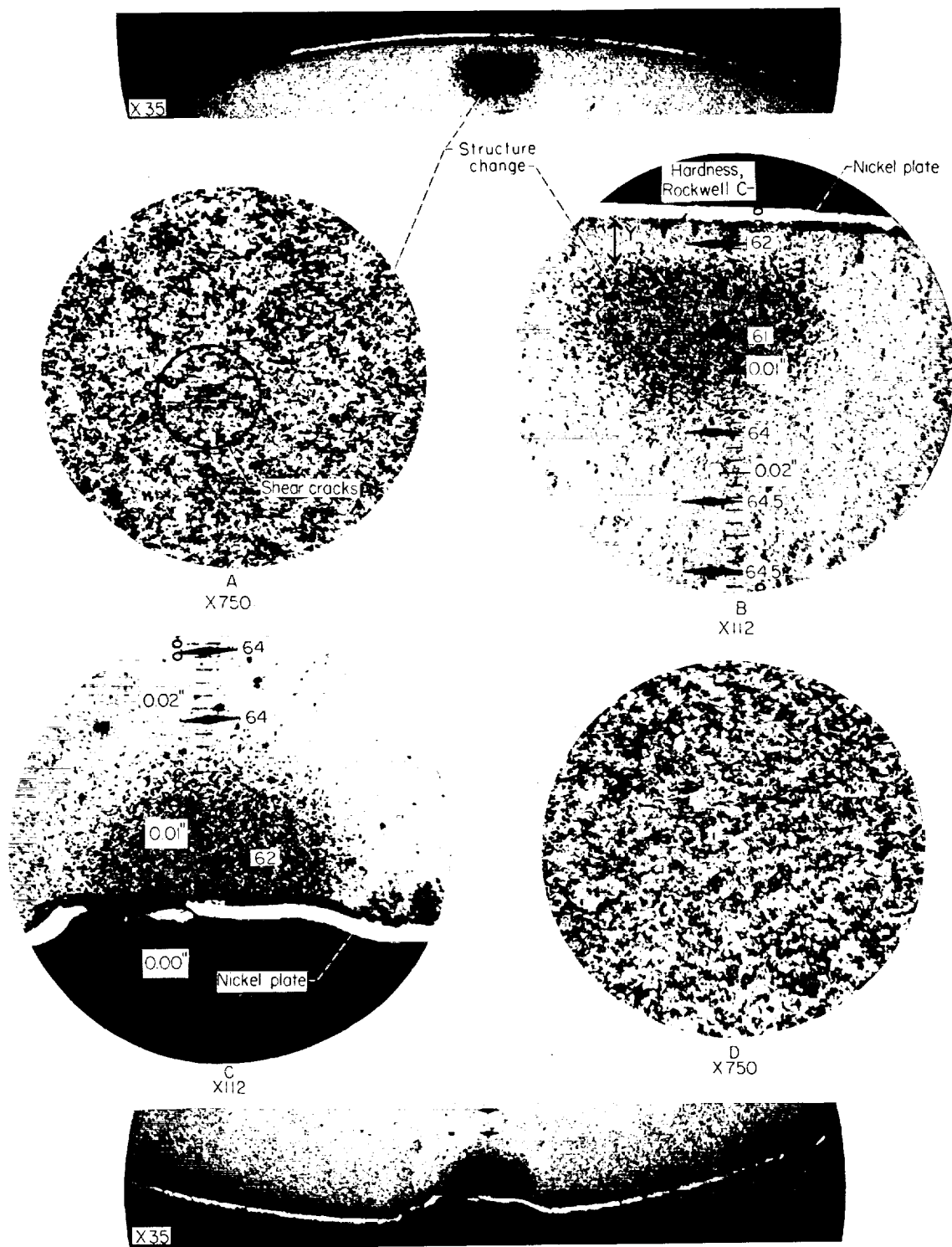FIGURE 31.—Structure change in SAE 52100 after $30\times10^6$ cycles at 250° F.   Longitudinal view.

FIGURE 32.—Structure change in SAE 52100 tested after $100 \times 10^6$ cycles at 250° F.   Transverse views.
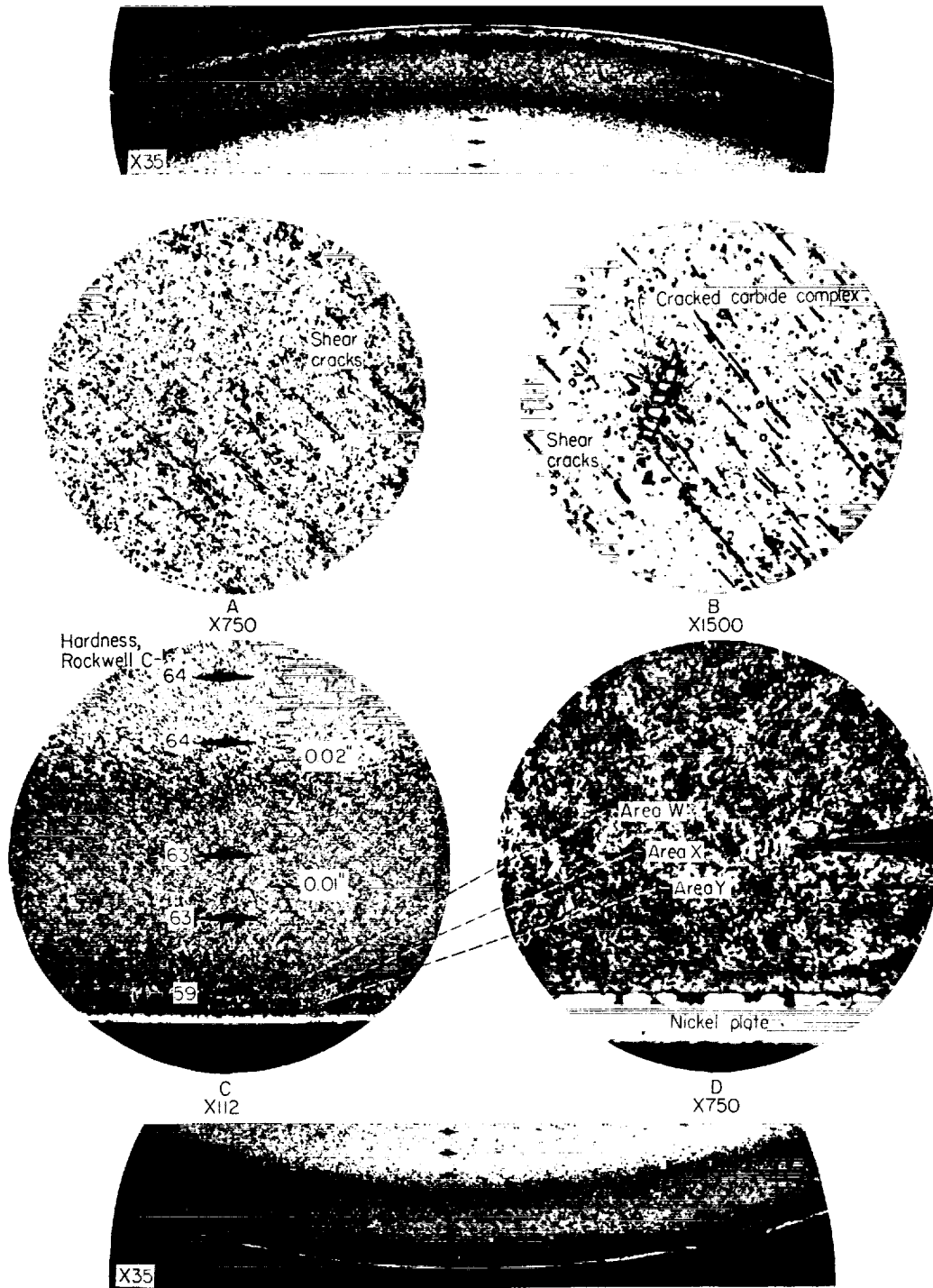
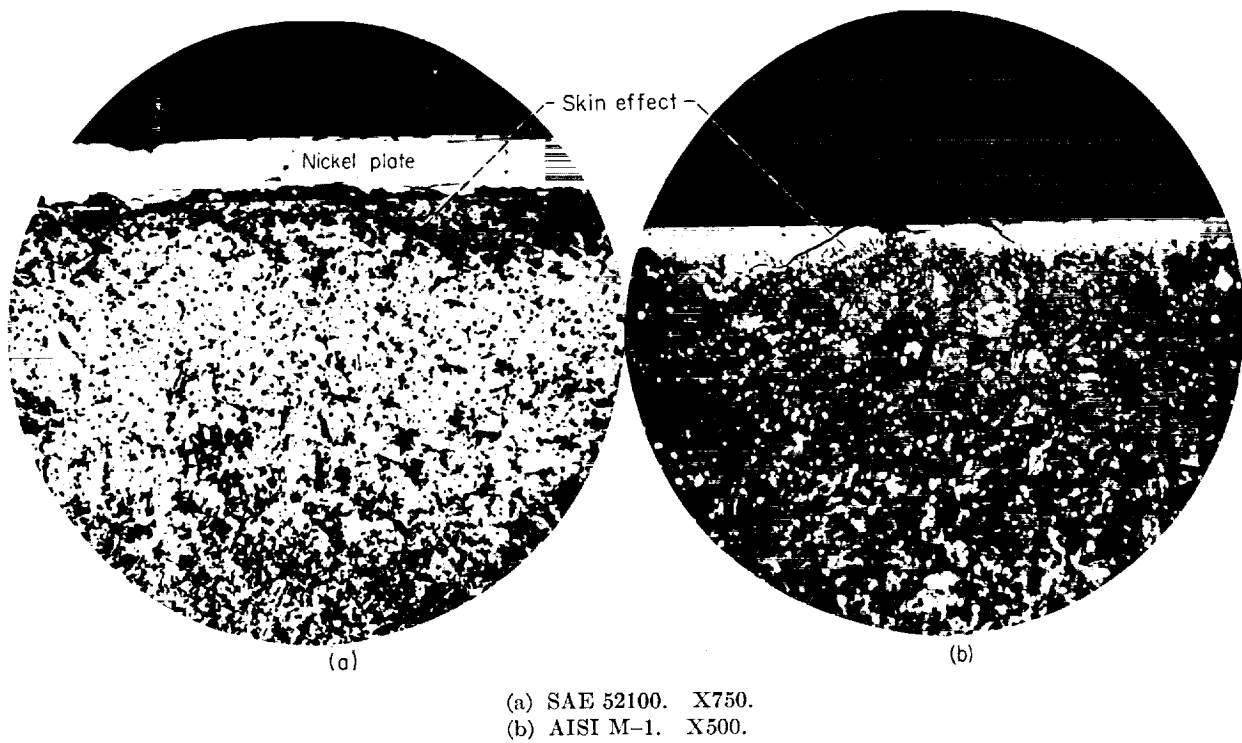FIGURE 33.—Structure change in SAE 52100 after $310 \times 10^6$ cycles at 250° F.   Longitudinal views.

(a) SAE 52100.   X750.
(b) AISI M-1.   X500.

FIGURE 34.—Cross sections showing skin effect.



(a) Crack.
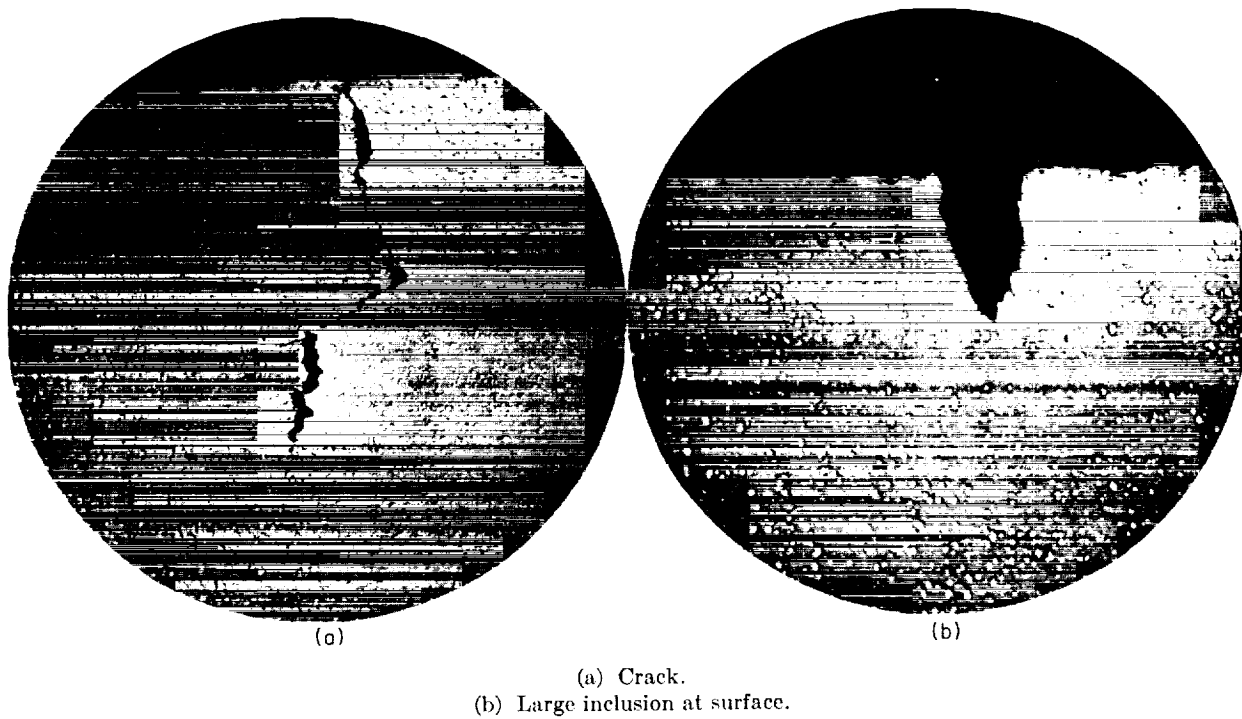(b) Large inclusion at surface.

FIGURE 35.—Defects on as-received AISI M-1 balls.   Unetched; X250.

deep, and its occurrence was erratic. Figure 34(a) shows an above-average case of such skin effects for SAE 52100 balls, and figure 34(b) shows a similar condition for AISI M–1. When pitting and wear occurred on the track, cracking developed as shown. Though the exact nature of the condition has not been determined, shear stresses due to the relative sliding of the rolling elements could affect this skin area in much the same manner as the high compressive load affects the subsurface area. Thus, the skin effect would depend on friction coefficients and rolling-element conformities as well as load. This effect may be much more
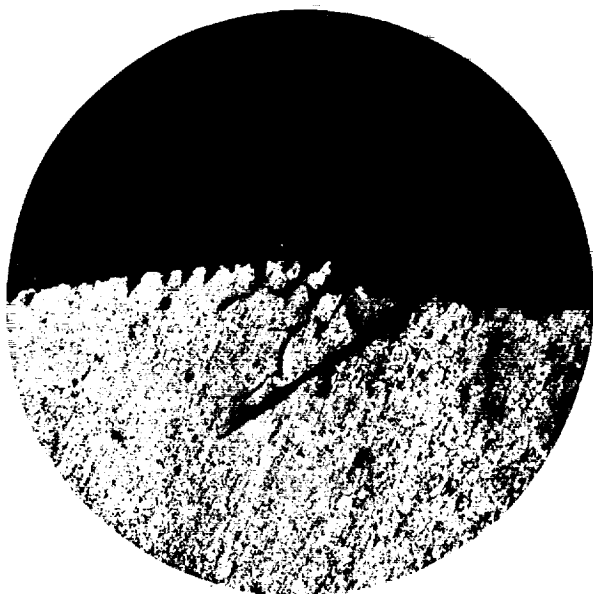


FIGURE 36.—SAE 52100 completed fatigue failure. Room-temperature test; X50.

pronounced in full-scale thrust bearings where relative sliding between contacting surfaces is much greater than in the spin rig.

**Origin and progression of fatigue failure.**—The sensitive shutoff mechanism in the spin rigs provided many small, incomplete failures for examination. Failures are not due to a single mechanism, even though there is a similarity in appearance and progression (spalling), as noted in the macroscopic investigation.

Very early failures (in less than $5 \times 10^6$ cycles) are believed caused by defective material not discernible by stringent preinspection. Several groups of balls were sectioned and examined in the as-received condition. Occasional defects,

generally in the pole areas, were found (such as shown in fig. 35).

Inclusions and their failure potentialities were previously discussed; yet very few completed failures that could be definitely attributed to inclusions were encountered. Either inclusions do not cause most failures, or the proof of damage is destroyed during the failure process. It was shown that inclusions are cracked and often crushed during fatigue testing, so that their retention even in an incomplete failure, such as shown in figure 9, is improbable. A large inclusion is only 0.001 inch in diameter, which is less than the width of the major cracks in a failure.

As mentioned earlier in the discussion, figure 9 shows the failure origin and progression of an SAE 52100, room-temperature, polar-area failure. Chemical segregation, parallel to the high compressive stresses, gives a structure inhomogeneity that can act as a metallurgical stress raiser or result in changes in elastic modulus. Secondary tensile stresses normal to the chemical segregation were believed to be too high, so that the fatigue crack indicated by A in figure 9 was generated. Shear cracks progressing from the original fatigue crack are shown by B. A completed failure of such origin is shown in figure 36. A slight variation, whereby failures initiate and progress in shear cracks, is given in figure 37(a), which shows the initial cracking and incipient spalling that follows.

Ball spalling averaged 0.005 inch in depth. Room-temperature SAE 52100 failures exhibited the deepest flake-outs and a more brittle type of cracking.

Typical SAE 52100 failures at 250° F were included in the photographs of figures 31 and 32. The partial failure in inset A of figure 31 appears to be representative of failure origin and initial propagation. No evidence that the structure change in the band took a direct part in these shallow failures was found in this investigation. However, these bands probably contributed indirectly to the failure by: (1) loss in strength, (2) internal stresses resulting from volume changes, and (3) a less ductile matrix layer between the ball surface and the troostitic band.

In AISI M–1 balls the fatigue failure mechanism was also shear. Figure 37(b) illustrates a failure at room temperature, and figures 37(c) and (d) are representative failures at 200° F. Again, fractures appear to be slightly more brittle at

(a)

(b)

(c)

(d)
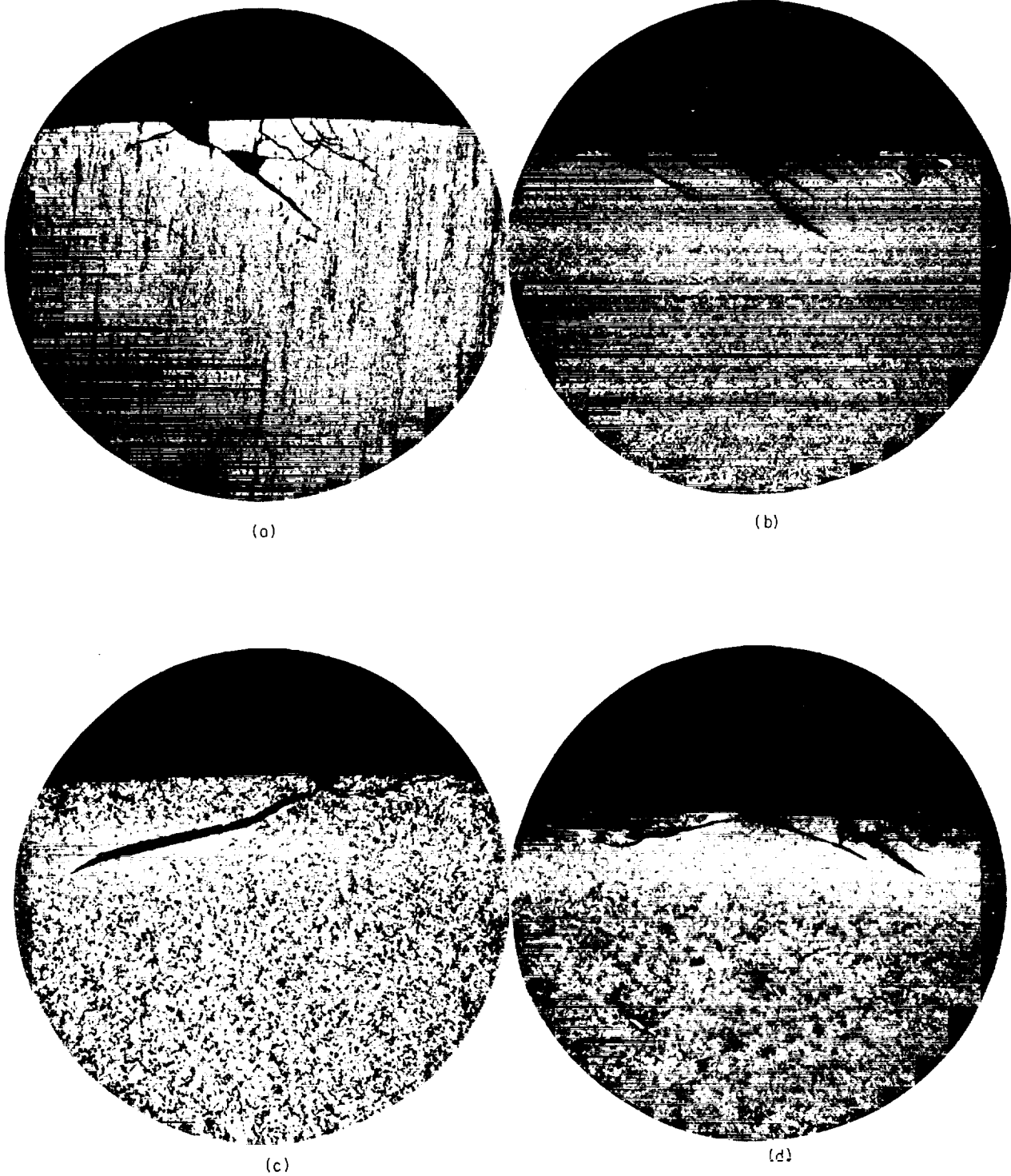
(a) SAE 52100 tested at room temperature.   X50.
(b) AISI M–1 tested at room temperature.   X50.
(c) AISI M–1 tested at 200° F.   X75.
(d) AISI M–1 tested at 200° F.   X50.

FIGURE 37.—Incompleted fatigue failures showing origin and progression in shear.

(a)

(b)

(c)

(d)

(a) Early stage of failure.  Unetched.
(b) Early stage of failure.  Etched.
(c) Late stage of failure.  Unetched.
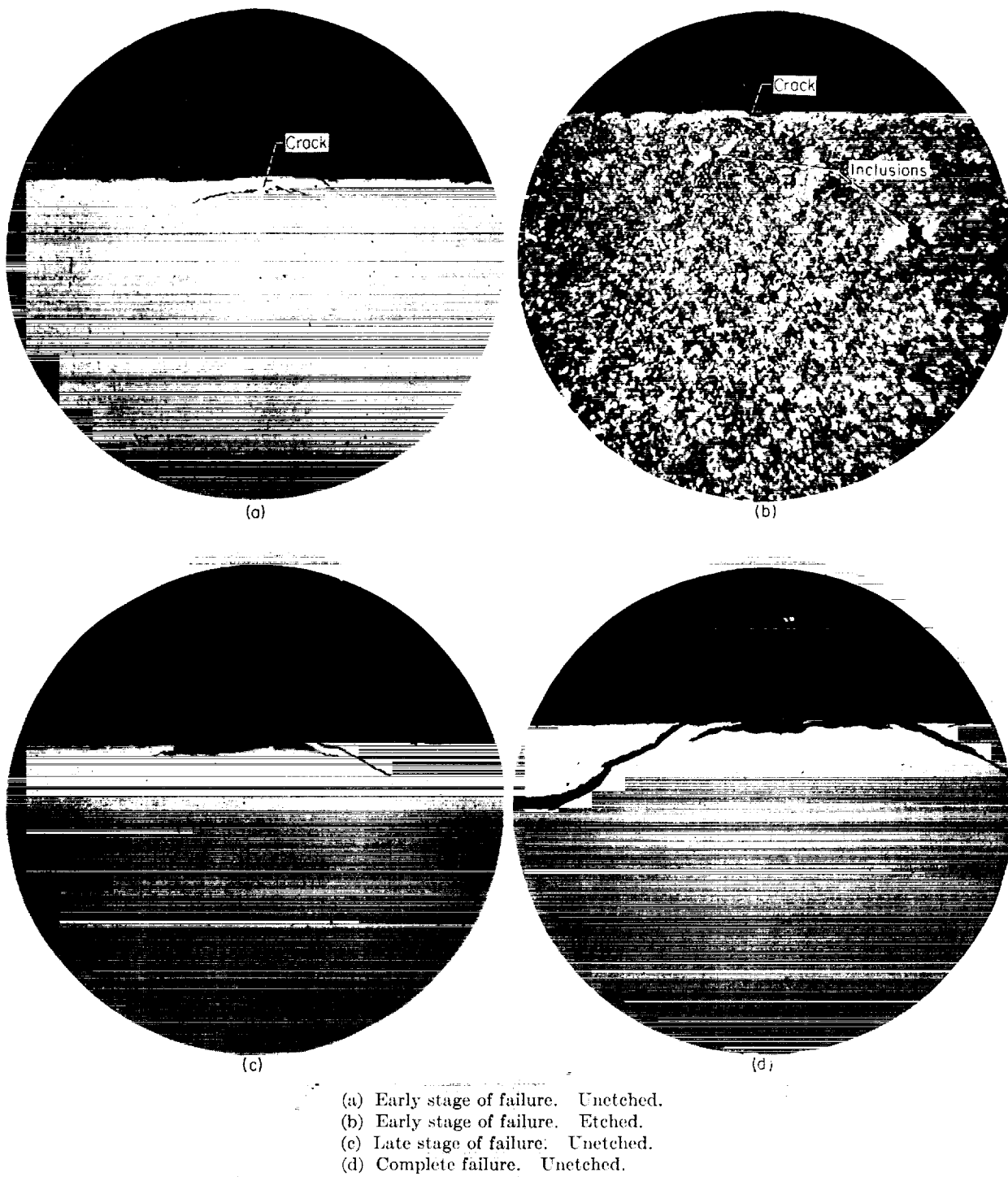(d) Complete failure.  Unetched.

FIGURE 38.--Origin and progression of fatigue failures caused by skin effects and track pitting in AISI M-1.  X250.

room temperature. Cracks are widest below the ball surface and penetrate into the band area. These views are sections through the ball equator and therefore show no fibrous structure.

When surface pitting or skin effects are prominent, fine subsurface cracks often occur, as shown in figure 38(a); (b) shows the same area etched. Initial small spalling can develop into a large failure; (c) and (d) show such a failure progression.

Failures originate within 0.005 inch of the ball surface and result primarily from shear cracking, although some failures indicated origin from secondary tensile stresses. Adverse surface conditions such as pitting or skin effects can also initiate a fatigue failure. The initial failure is a very small spall such as pictured in figure 37(a), which also shows the failure progression.

Hardness.—Many Tukon hardness surveys were made. A few of these are included with the photomicrographs used in the preceding discussions. Rockwell C equivalents are given in place of the Knoop hardness numbers. These hardness studies were less decisive than expected, many hardness trends falling within the error margin of testing. Carbides prevented obtaining true matrix hardness values. A summary of hardness testing is as follows:

(1) No decisive hardness differences were indicated between the as-received and the endurance-tested balls.

(2) The troostitic bands in SAE 52100 showed a slight hardness decrease but not as great a decrease as the change in structure would indicate.

(3) In the banded areas in the AISI M-1 balls, hardness values were indecisive, although slight hardness-increase trends were indicated in some of the more severely banded balls.

(4) The skin effects in AISI M-1 steel, in the few places deep enough to be tested, showed softening.

(5) It can be observed on the photomicrographs that the first hardness value next to the ball surface indicates softening. This same effect was found on as-received balls and is apparently an edge effect, since these balls when tested at light loads showed no softening. In long-run balls, however, light-load hardness values indicated that slight softening took place.

### ALLOY COMPOSITION

As a preliminary evaluation of the effect of alloy composition, groups of balls having different analyses (table I) were run under rolling-contact fatigue conditions at room temperature with an SAE 10 paraffinic-base mineral oil lubricant (table II). All data presented are for a loading that produces a maximum theoretical Hertz stress of 725,000 psi at the surface and 225,000 psi in shear 0.009 inch below the contact surface. A comparison is included of AISI M-1 vacuum- and air-melt heats that were run under the same test conditions, except that the lubricant was a water-soluble polyalkylene glycol. Since all materials used had a cleanliness rating of A-1 and D-1 or better on the Jernkontoret chart, a more sensitive cleanliness evaluation was obtained by assigning each material to one of three arbitrary subratings within the A-1 and D-1 specification.

Results.—A summary of the Weibull plots for these tests is presented in graphic form in figure 39.

Discussion.—An important consideration in interpreting these results is the fact that only one heat of each material was tested. Wide variations in properties can occur between two heats of the same nominal alloy composition. Some of these variations, such as cleanliness and residual elements, may have a very important bearing on fatigue life performance. The results presented herein are, therefore, considered preliminary.

Beneficial effects were observed with vacuum melting. A group of vacuum-melted AISI M-1 balls showed a significant increase in life over a group of air-melted AISI M-1 balls run at the same test conditions. The improvement was of the order of magnitude of 10 to 1. The vacuum-melted balls were rated as excellent in cleanliness, while the air-melted balls were rated as fair. A similar increase in fatigue life was observed with AISI M-1 race specimens.

Tests were made of SAE 52100 base alloys that were modified by aluminum and silicon additions with or without molybdenum modification. The results for these two materials, MHT and TMT, showed an improvement over standard SAE 52100. The alloy MHT had about 1 percent aluminum added, and TMT had 1 percent silicon content. With the addition of these deoxidizers, fewer short-lived failures were obtained, and the scatter in life was reduced. All three groups of specimens, which were of the same
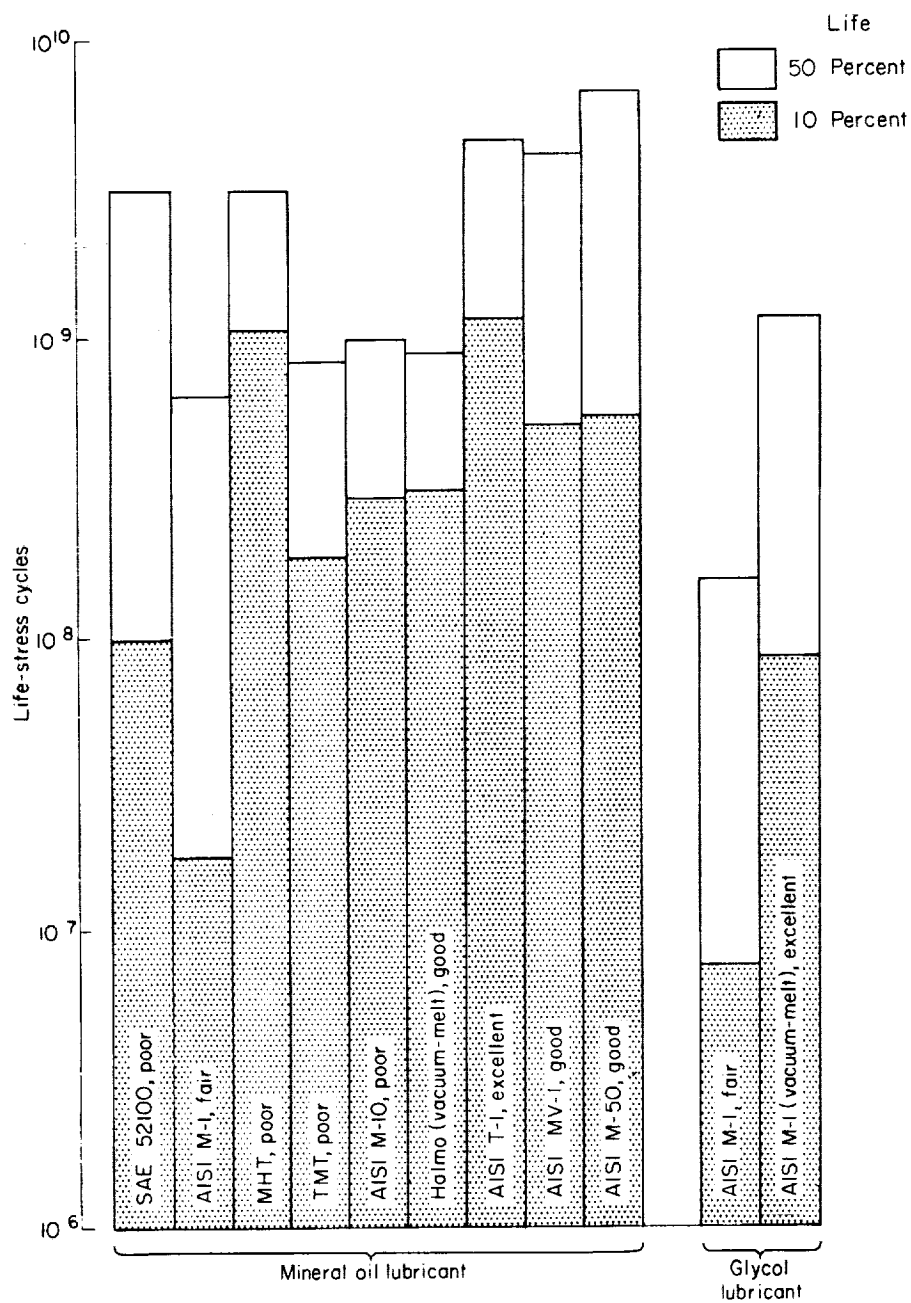
FIGURE 39.—Summary of ball life data giving material and cleanliness ranking within A-1 and D-1 Jernkontoret ratings.

cleanliness, were rated as poor within the ASTM A-1 and D-1 classifications.

No correlation of fatigue life with cleanliness was obtained for the various specimens. The effect of the different alloy compositions may have been large enough to obscure any definite correlation, if such correlation did exist.

## SUMMARY OF RESULTS

A series of investigations was made in the fatigue spin rig to evaluate the effect on rolling-contact fatigue life of stress, forging fiber orientation, lubricant viscosity, lubricant base stock, temperature, dry-powder lubricants, metallurgical structure, and alloy composition. Ball specimens of ½- and ⁵⁄₁₆-inch diameter were tested at loads producing maximum theoretical Hertz stresses in the range of 600,000 to 750,000 psi compression. Results are as follows:

1. Contact stresses resulting from applied load affected rolling-contact fatigue life. Life varied inversely as the tenth power of stress; this is in good agreement with values accepted by the bearing industry as representative of full-scale bearing assemblies.

2. The orientation of forging fibers at the contacting surface was found to have an important effect both on location of failure and on life. Those areas having the highest angle of intersection of the forging fiber with the contact surface had a greater propensity for failure and shorter fatigue life than areas in the same specimen that had fiber approximately parallel to the contact surface. A continuous trend in both life and failure density was observed for fiber angles between the two extremes. The effect of fiber orientation angle appeared to be independent of alloy composition for the nine alloys investigated.

3. Higher lubricant viscosity produced longer fatigue lives. A life ratio of 2 to 1 was observed between paraffinic lubricants of 120 and 5 centistokes, respectively. Intermediate viscosities indicated that a continuous upward trend existed.

4. Lubricants of different base stock produced wide variances in fatigue life. Five fluids having the same viscosity at 100° F produced a life ratio from best to poorest of 40 to 1. The rate at which actual viscosity increased with high pressure (of the magnitude existing in the contact zone)

correlated well with life results. Chemical activity of the five different fluid lubricants did not appear to produce a significant effect on fatigue life.

5. Increasing temperature produced lower fatigue life. This reduction was greater than that anticipated from temperature-lowering of lubricant viscosity. Metallographic structural changes in the subsurface zone of maximum shear stress were observed. The intensity of these structural changes increased with the number of stress cycles and was accelerated by higher temperature.

6. Dry-powder lubricants produced low fatigue life at 450° F. Chemical activity of the powder lubricant did not appear to have a significant effect on fatigue life. Failure appearance indicated that minute stress raisers, probably the lubricant particles themselves, produced localized accelerated failures in the bands of pure rolling. This effect should not be as pronounced in full-scale bearings that have greater amounts of sliding in the contact zone.

7. Nonmetallic inclusions in the subsurface zone of high shear stress were found to have an adverse effect on fatigue life. Inclusion size, location, and composition as well as the condition of the surrounding matrix were important contributing factors. The inclusions acted as stress raisers and promoted plastic deformation and microscopic cracking of the surrounding matrix. Most failures originated with subsurface cracking that increased in magnitude and eventually produced the shallow spall characteristic of rolling-contact fatigue failures.

8. Based on limited data obtained with one heat each of the air-melt and vacuum-melt AISI M-1 steel, vacuum melting improved fatigue life by a factor of 10 to 1. However, a general correlation between cleanliness and fatigue life in all materials studies was not obtained.

9. Life results from one heat each of ten different materials are presented. Deoxidizers appeared to improve standard SAE 52100 steel with respect to fatigue life, although conclusions based on single heats of material are not considered adequate to evaluate a particular alloy.

Lewis Research Center
National Aeronautics and Space Administration
Cleveland, Ohio, *June 16, 1959*

## REFERENCES

1. NACA Subcommittee on Lubrication and Wear: Review of Current and Anticipated Lubricant Problems in Turbojet Engines. NACA RM 51D20, 1951.

2. Perlmutter, Isaac: Rolling Contact Bearings for High Temperature Applications. Memo. Rep. WCRTL–M–5620, Materials Lab., Res. Div., WADC, Apr. 15, 1952.

3. SAE Panel on High-Speed Rolling-Contact Bearings: Trends of Rolling-Contact Bearings as Applied to Aircraft Gas-Turbine Engines. NACA TN 3110, 1954.

4. Barnes, Gilbert C., and Ryder, Earle A.: A Look at Some Turbine Bearing Problems. Preprint No. 693, SAE, 1956.

5. Epremian, E., and Mehl, R. F.: Investigation of Statistical Nature of Fatigue Properties. NACA TN 2719, 1952.

6. Styri, Haakon: Fatigue Strength of Ball Bearing Races and Heat-Treated 52100 Steel Specimens. Proc. ASTM, vol. 51, 1951, pp. 682–700.

7. Lundberg, G., and Palmgren, A.: Dynamic Capacity of Rolling Bearings. ACTA Polytech., Mech. Eng. Ser., vol. 1, no. 3, 1947.

8. Macks, E. F.: The Fatigue Spin Rig—A New Apparatus for Rapidly Evaluating Materials and Lubricants for Rolling Contact. Lubrication Eng., vol. 9, no. 5, Oct. 1953, pp. 254–258.

9. Jones, A. B.: New Departure—Analysis of Stresses and Deflections. Vols. 1 and 2. New Departure, Div. General Motors Corp., Bristol (Conn.), 1946.

10. Johnson, Leonard G.: The Median Ranks of Sample Values in Their Population With an Application to Certain Fatigue Studies. Ind. Math., vol. 2, 1951, pp. 1–9.

11. Grover, H. J., Gordon, S. A., and Jackson, L. R.: Fatigue of Metals and Structures. NAVAER 00–25–534, Dept. Navy, Bur. Aero., 1954.

12. Johnson, Leonard G.: The Statistical Treatment of Fatigue Experiments. GMR 202, Res. Labs., General Motors Corp., Apr. 1959, pp. 44–47.

13. Anderson, W. J., and Carter, T. L.: Effect of Fiber Orientation, Temperature, and Dry Powder Lubricants on Rolling Contact Fatigue. ASLE Trans., vol. 2, no. 1, Apr. 1959, pp. 108–120.

14. Otterbein, Mark E.: Effect of Aircraft Gas Turbine Oils on Roller Bearing Fatigue Life. Paper No. 57–LC–9, ASLE, 1957.

15. Jones, A. B.: Metallographic Observations of Ball Bearing Fatigue Phenomena. Symposium on Testing of Bearings, ASTM 1947, pp. 35–48; discussion, pp. 49–52.

16. Barwell, F. T., and Scott, D.: Effect of Lubricant on Pitting Failure of Ball Bearings. Engineering, vol. 182, no. 4713, July 6, 1956, pp. 9–12.

17. Anon.: Viscosity and Density of Over 40 Lubricating Fluids of Known Composition at Pressures to 150,000 PSI and Temperatures to 425° F. Vol. II. ASME, 1953.

18. Lieblein, Julius: A New Method of Analyzing Extreme-Value Data. NACA TN 3053, 1954.

19. Dorr, J.: Schmiermitteldruck und Randverformungen des Rollenlagers. Ing.-Archiv., Bd. XXII, 1954, pp. 171–193.

20. Cordiano, H. V., Cochran, E. P., Jr., and Wolfe, R. J.: A Study of Combustion Resistant Hydraulic Fluids as Ball Bearing Lubricants. Lubrication Eng., vol. 12, no. 4, July–Aug. 1956, pp. 261–266.

21. Charron, Fernand: Viscosite sous pression rapidement variable. Paris Inst. Francais du petrole. Revue, t. 4, no. 1, Jan. 1949, pp. 3–14.